MP100276

MITRE PRODUCT

MITRE

Independent Control Segment URA Monitor for GPS IIIC with Application to LPV200

Ronald Braff
Brian Bian
Curtis Shively

September 2010

CAASD

MP100276

MITRE PRODUCT

MITRE

Independent Control Segment URA Monitor for GPS IIIC with Application to LPV200

Ronald Braff
Brian Bian
Curtis Shively

September 2010

Sponsor: The Federal Aviation Administration
Dept. No.: F046
Project No.: 0210EA03-MP
Outcome No.: 3
PBWP Reference: 3-7.A-1
"Report on GPS III Integrity and Continuity Assurance"

Abstract

To assure the integrity of critical navigation operations, the user range accuracy (URA) is envisioned to provide future GPS IIIC users the means to rigorously bound the fault-free and fault-induced errors that may be contained in the signal-in-space (SIS) from each space vehicle (SV). This paper examines an independent URA monitor (IUM) that could be incorporated into the next generation GPS Control Segment (OCX) to assure that the broadcast URA bounds any errors in the broadcast SV ephemeris and clock correction parameters. The proposed IUM estimates these errors based on the difference between the SV position computed using the broadcast parameters and the SV position computed using range measurements from receivers located at the worldwide GPS monitor stations (MSs). The IUM applies a threshold test to the projection of the estimated errors onto the SV line-of-sight for each assumed user located at a set of grid points in the SV footprint. The IUM output is either a computed minimum monitorable URA (MMU) or an alert if there is a threshold violation at any assumed user grid point. The magnitude of the MMU is based on the quality of the IUM measurements. The IUM operates on single or multiple snapshot data in order to maintain an independent and timely integrity assured URA for each OCX upload to an SV. It thus generates larger URAs than would be obtained when they are generated from continuous tracking data and an orbital model. A performance assessment, based on an example GPS IIIC constellation and covariance analysis, is used to estimate the worldwide magnitudes of the MMUs generated by the IUM.

To examine operational feasibility of the IUM, an analysis is presented for an application of GPS IIIC with IUM to the stringent integrity requirements of the Localizer Performance with Vertical guidance (LPV) aircraft approach operation down to a 200 ft decision altitude (LPV200). In this application, for the position error bounding to be feasible, the distribution of the errors contained in each range measurement (GPS IIIC SIS + airborne) used in the position solution has to be bounded by a normal error distribution. This requirement is addressed as part of the LPV200 application analysis. Although the IUM may produce MMUs that are somewhat larger than the URAs previously envisioned for GPS IIIC, the analysis of the LPV200 operation indicates sufficiently high availability at U.S. locations, including Alaska and Hawaii. Analysis of several non-U.S. locations indicates availability values less than 0.99 and significant loss of availability in the Southern Hemisphere.

Table of Contents

List of Figures

List of Tables

1 Introduction

1.1 Overview

The user range accuracy (URA) is a parameter in the GPS space vehicle (SV) broadcast message. Its purpose is to provide the means to bound the errors in the SV signals-in-space (SIS). These errors include nominal (fault-free) and fault-induced ephemeris, clock[1] and signal distortion errors. In a user's receiver, URA is combined with standard deviations of other errors (e.g., user receiver errors and residual troposphere error) to estimate bounds on the ranging errors. These range error bounds are the inputs for the computation of an error bound for a user's position solution. For high integrity applications the position error needs to be bounded with high probability (on the order of $1 - 10^{-7}$).

GPS III, comprising Block III satellites and the next generation operational control system (OCX), is intended to have the potential to support such high integrity applications, without additional ground augmentation. A general discussion of the GPS III integrity concept may be found in [1]. For Block IIIA and IIIB satellites the level of integrity is intended to match the "legacy" level of $1 - 10^{-5}$ / h per SV for SIS. However, with Block IIIC satellites an "assured" integrity level of $1 - 10^{-8}$ / h per SV for SIS will be provided if the integrity status flag (ISF) is "on". Several methods for achieving such a high level of assured integrity are included in the GPS III integrity concept [1]. First, GPS III satellites will have the capability to detect clock faults or other on-board processing anomalies and rapidly switch the output signal to an untrackable non-standard code. Second, the OCX will take steps to assure that bad clock and ephemeris prediction data and URA data are not uploaded to a satellite. Of course the OCX will still also observe, estimate and correct slow drift satellite clock errors and ephemeris errors that may not be detectable by satellite on-board monitoring as is done by the current control segment.

The GPS III integrity concept as described in [1] is directed at addressing the two most significant integrity threats previously identified as satellite clock faults and bad data uploaded by the ground control system. However, there may be residual risks of other integrity failure modes that are large enough to require some additional mitigation. Furthermore, an independent SIS monitor may be needed, as in the FAA's Wide Area Augmentation System (WAAS), since approval authorities may not accept integrity parameters that are not independent of the process that generates the ephemeris and clock correction broadcast message.

This paper examines the incorporation of an independent URA monitor (IUM) as one of the functions of the OCX that assures the broadcast URA bounds the ephemeris and clock errors according to the GPS IIIC assured integrity specification. The IUM does not monitor other SIS errors, such as signal distortion, which would require a separate monitor. The IUM is a process that estimates ephemeris and clock errors independently from the OCX estimation process, using separate algorithms and computers, and possibly separate monitor receivers. The error estimation is based on the difference between the SV position and clock solution based on the

[1] The SV broadcast data includes parameters for computing the SV clock correction. In this paper "clock error" refers to the residual clock error after application of the clock correction based on these broadcast parameters.

broadcast ephemeris and clock correction data and the SV position and clock solution derived from range measurements from receivers located at the worldwide GPS monitor stations (MSs). The method of error estimation is by least squares from single and multiple snapshot measurements. Since URA is an OCX generated upload parameter, it would be refreshed by the OCX every 15 min. Therefore, the IUM has to operate in the 15 min interval between OCX uploads.

The purpose of this paper is to illustrate the impact of an IUM on the magnitude of the broadcast URA and investigate the performance of GPS IIIC with an IUM, as part of the OCX, in meeting the integrity requirements of the Localizer Performance with Vertical Guidance (LPV) 200 (200 ft decision altitude) aircraft approach operation. Since LPV200 has stringent integrity requirements, the ability to satisfy these requirements provides an initial assessment of the operational feasibility of an IUM.

The IUM described herein is one approach to determining a high integrity URA. Other approaches, such as combining ground-based pseudorange measurements with space-based pseudorange measurements obtained through cross-link ranging, may provide additional improvements, but are beyond the scope of this study.

1.2 Contents

The rest of the paper is divided into the following five sections.

Description of IUM: This section contains a description of the monitor process, including the minimum monitorable URA (MMU), the IUM's output for each SV when there is no threshold violation.

IUM Performance Model: This section includes the IUM measurement threshold definitions and assumptions used in the performance analysis.

MMU Results: This section contains MMU computations in both worldwide graphical and specific location tabular percentile formats.

Application to LPV200: The integrity availability of LPV200 is presented at representative U.S. locations and several selected worldwide locations.

Appendices: There are three appendices containing: A) assumed IUM measurement error model, B) fault-free ephemeris and clock error covariance model and C) an analysis of bounding the SV broadcast ephemeris and clock error distribution, including its dependence on a priori SV fault rate.

2 Description of IUM

2.1 IUM Overview

The objective of the IUM is to provide an independent check that 5.73 URA bounds an SV's ephemeris and clock broadcast errors with probability 10^{-8} per h with respect to fault-free and fault-induced errors. Figure 1 contains a flow chart of the IUM process.

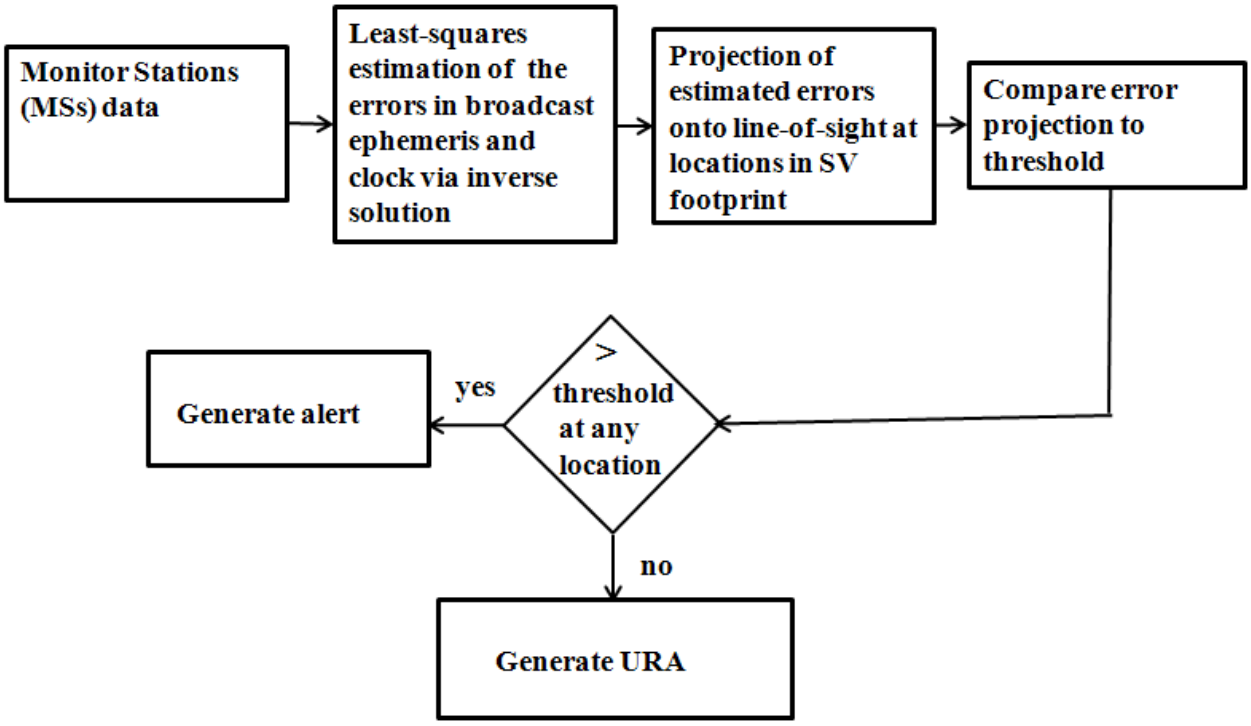

Figure 1 IUM Process

A range error estimate (δr_m) for each SV is formed as

$$\delta_{rm} = r_{m\_calc} - r_{m\_meas} \quad (1)$$

r_{m_calc}: calculated range based on SV broadcast ephemeris and exact location of MS_m

r_{m_meas}: measured range based on broadcast SV clock correction and MS clock (MS clocks are assumed to be perfectly synchronized)

The δr_m are the inputs to the SV position and clock error estimation solution (δ**e**) which is expressed as

$$\delta\mathbf{e} = \begin{bmatrix} \delta e_h \\ \delta e_c \\ \delta e_l \\ \delta e_t \end{bmatrix} = \begin{bmatrix} h_b \\ c_b \\ l_b \\ t_b \end{bmatrix} - \begin{bmatrix} \hat{h} \\ \hat{c} \\ \hat{l} \\ \hat{t} \end{bmatrix} \quad (2)$$

h_b, c_b, l_b, t_b : SV position and clock solution based on broadcast parameters coordinates

$\hat{h}, \hat{c}, \hat{l}, \hat{t}$: SV position and clock solution based on MS measurements and precise knowledge of MS antenna phase center coordinates

$\delta\mathbf{e}$ is projected onto the line-of-sight at grid points in the SV footprint

$$\delta e_{i,k\_proj} = \mathbf{L}_{i,k}^{T} \bullet \delta\mathbf{e} \quad (3)$$

$\delta e_{i,k\_proj}$: decision statistic at location i, k

i, k: spherical angle grid coordinates

$\mathbf{L}_{i,k}$: line-of-sight unit vector from a grid point i, k in the SV footprint

$\delta e_{i,k\_proj}$ are the decision statistics that are compared to monitor threshold values ($T_{i,k}$) at the grid-points. If any $\delta e_{i,k\_proj} > T_{i,k}$, an alert is generated; otherwise a URA value is calculated for uplink to the SV for broadcast. The IUM computes a minimum monitorable URA (MMU). The uplinked URA for broadcast is URA $\geq \max\{URA_{pm}, MMU\}$, where URA_{pm} is the URA computed by the OCX prior to the monitor. The reason for the inequality is explained below.

2.2 Monitor Threshold

The threshold ($T_{i,k}$) is calculated at each grid point

$$T_{i,k} = k_T \sqrt{\sigma_{i,k\_meas}^2 + \sigma_{i,k\_ure}^2} \quad (4)$$

k_T: threshold multiplier that sets false alert rate

σ_{i,k_meas}: standard deviation of the errors in IUM estimation of ephemeris and clock when projected onto grid coordinate line-of-sight

σ_{i,k_ure}: standard deviation of fault-free errors in SV ephemeris and clock broadcast when projected onto grid coordinate line-of-sight

Note that $\sqrt{\sigma_{i,k\_meas}^2 + \sigma_{i,k\_ure}^2}$ represents the decision statistic standard deviation over the SV footprint in the absence of fault induced errors.

2.3 MMU Concept

MMU is the minimum value of URA for which the required probability of loss of integrity given the presence of a fault (P_{LOIGF}) does not exceed a required value, P_{LOIGF_req}. That is,

$$P_{LOIGF} = \text{Prob}\{|\varepsilon_{act}| > 5.73 \text{ MMU} \mid \text{fault}\} \le P_{LOIGF\_req} \quad (5)$$

ε_{act}: component of user's actual range measurement error due to errors contained in the SV SIS (e.g, ephemeris and clock errors)

P_{LOIGF_req} is defined as

$$P_{LOIGF\_req} = \frac{P_{alloc}}{P_{fault}} \quad (6)$$

P_{alloc}: fault-tree allocation per h for the risk of 5.73 URA not bounding URE due to a fault-induced error

P_{fault}: a priori probability of a fault per h. For example, if $P_{alloc} = 10^{-8}$ / h and $P_{fault} = 10^{-4}$ / h, $P_{LOIGF\_req} = 10^{-4}$

Referring to (5), it is seen that if the pre-monitor URA computed by the OCX (URA_{pm}) were smaller than MMU then P_{LOIGF} could exceed P_{LOIGF_req}. However, for this IUM concept, MMU only reflects SV ephemeris and clock integrity. Therefore, URA_{pm} could be > MMU due to the OCX mitigating other fault modes, such as signal deformation. The assurance of the integrity of other fault modes is beyond the capability of this IUM since its decisions are based only on range measurements. Therefore, the broadcast URA would have to be

$$URA \ge \max\{URA_{pm}, \text{MMU}\} \quad (7)$$

2.4 MMU Definition

Two formulations of MMU have been defined. They are the monitor model formulation (MMU_{model}) and the protection level formulation (MMU_{PL}). The definitions and comparison of the two formulations are given below.

2.4.1 MMU_{model}

The following parameters are used in deriving MMU_{model}.

m: measurement error contained in decision statistic in (3) at a grid point

σ_{meas}: standard deviation of m

e: fault-free SV broadcast error (ephemeris and clock) contained in decision statistic at a grid point

σ_{ure}: standard deviation of e

$s = m + e$

b: fault-induced error in SV broadcast contained in decision statistic at a grid point

The location of the peak of a fault-induced error is unknown over the SV footprint. Therefore, the greatest risk of loss-of-integrity occurs at the maximum threshold location. MMU_{model} is computed at this location where $T_{max} = \max\{T_{i,k}\}$. Loss of integrity for a user at the same location as T_{max} is expressed as

$$|e+b| > K_I MMU \cap |s+b| \le T_{max} \tag{8}$$

K_I: multiplier corresponding to required probability of loss of integrity

Assuming normal distribution of fault-free errors, the MMU_{model} formulation is defined as the probabilistic representation of (8)

$$P_I(U,b) = \int_{K_I U-b}^{\infty} \int_{-T_{max}-b}^{T_{max}-b} f(s,e)\,ds\,de + \int_{-\infty}^{-K_I U-b} \int_{-T_{max}-b}^{T_{max}-b} f(s,e)\,ds\,de \tag{9}$$

$$f(\varepsilon,e) = \frac{1}{2\pi\sqrt{\det(c)}} \exp\left(-0.5 \begin{bmatrix} s & e \end{bmatrix} c^{-1} \begin{bmatrix} s \\ e \end{bmatrix}\right) \tag{10}$$

$$c = \begin{bmatrix} \sigma_{meas}^2 + \sigma_{ure}^2 & \sigma_{ure}^2 \\ \sigma_{ure}^2 & \sigma_{ure}^2 \end{bmatrix} \tag{11}$$

$$MMU_{model} \text{ satisfies } \underset{b}{peak}\{P_I(MMU_{model}, b)\} = P_{LOIGF\_req} \tag{12}$$

It can be shown that there is only one pair of values of $U = MMU_{model}$ and b that satisfies (12).

2.4.2 MMU_{PL}

MMU_{PL} is an intuitive and simpler definition of MMU. It is based on assuming that P_{LOIGF} equals the probability of missed detection (P_{md}). P_{md} is defined as the probability that the IUM measurement error hides a threshold violation due to a fault induced error.

$$P_{i,k\_md}(\varepsilon+b) = \int_{-T_{i,k}-(\varepsilon+b)}^{T_{i,k}-(\varepsilon+b)} g(m)\,dm \tag{13}$$

$$g(m) = \frac{1}{\sqrt{2\pi}\,\sigma_{i,k\_meas}} \exp\left(-\frac{m^2}{2\,\sigma_{i,k\_meas}^2}\right) \tag{14}$$

The protection level bound is defined as

$$5.73\,MMU_{i,k} \ge T_{i,k} + K_{md}\,\sigma_{i,k\_meas}, \text{ all footprint locations} \tag{15}$$

$$MMU_{PL} = peak\left\{\frac{T_{i,k} + K_{md}\,\sigma_{i,k\_meas}}{5.73}\right\} \tag{16}$$

$$P_{md}(5.73\,MMU_{PL}) = \int_{-T_{max}-5.73\,MMU_{PL}}^{T_{max}-5.73\,MMU_{PL}} g(m)\,dm \tag{17}$$

K_{md}: multiplier chosen via an iterative solution to make $P_{md}(5.73\,MMU_{PL}) = P_{LOIGF\_req}$

2.4.3 Selection of URA Definition

Due to ease of MMU_{PL} computation and $MMU_{PL} \geq MMU_{model}$, MMU_{PL} is the output of the IUM. Referring to (9), proving that peak$\{P_I(MMU_{PL}, b)\} \leq P_{LOIGF_req}$ is equivalent to proving that $MMU_{PL} \geq MMU_{model}$.

$$P_I(MMU_{PL}, b) = \int_{5.73\,MMU_{PL}-b}^{\infty} \int_{-T_{max}-b}^{T_{max}-b} f(e, s)\,ds\,de \tag{18}$$

Since e and m are independent and the monitor decision statistic s = e + m,

$$P_I(MMU_{PL}, b) = \int_{5.73\,MMU_{PL}-b}^{\infty} \int_{-T_{max}-(e+b)}^{T_{max}-(e+b)} g_e(e)\,g_m(m)\,dm\,de. \tag{19}$$

The inner integral is the definition of $P_{md}(e + b)$ (13) and the range of the outer integral is $e \leq 5.73\ MMU_{PL} - b$ implying that $(e + b) \leq 5.73\ MMU_{PL}$. Therefore, referring to (17), the inner integral $\geq P_{LOIGF\_req}$.

$$P_I(MMU_{PL}, b) \leq P_{LOIGF\_req} \times \int_{5.73MMU_{PL}-b}^{\infty} g_e(e)\,de \leq P_{LOIGF\_req} \tag{20}$$

Since

$$\int_{5.73MMU_{PL}-b}^{\infty} g_e(e)\,de \leq 1 \tag{21}$$

It was shown by several different examples that MMU_{PL} is also slightly > MMU_{model} so that MMU_{PL} is a good approximation to the more rigorous MMU_{model}. An example of the two definitions of MMU is shown in Figure 2. In Figure 2, $P_{LOIGF\_req} = 10^{-4}$, based on the assumptions that $P_{alloc} = 10^{-8}$ / h, $P_{fault} = 10^{-4}$ / h in (6).

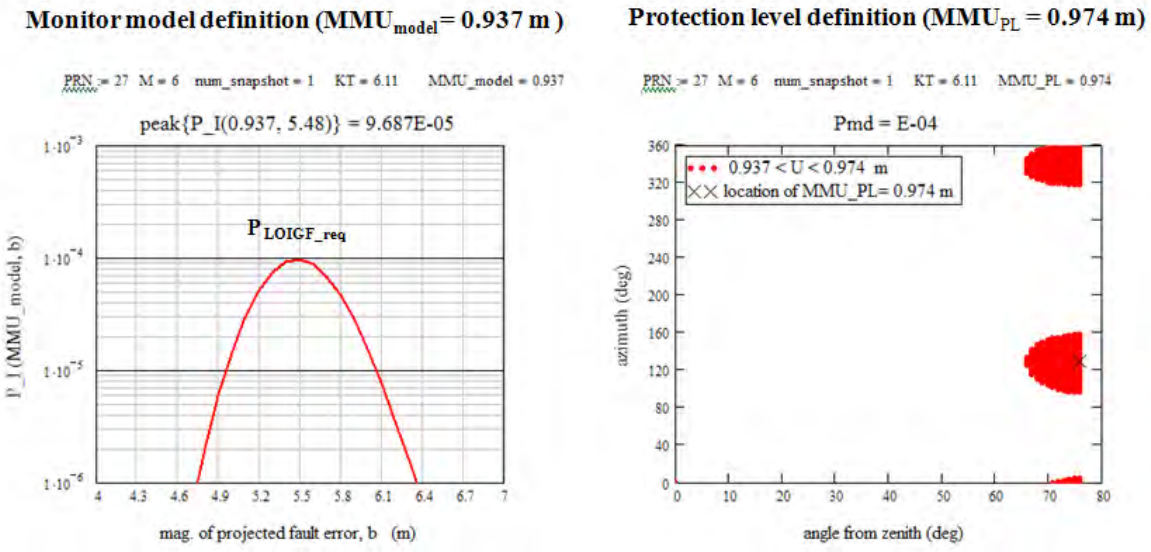

Figure 2 Example of Two Definitions of MMU

Since it has been shown that $P_I(MMU_{PL}, b)$ is always $\leq P_{LOIGF\_req}$ then 5.73 MMU_{PL} bounds any magnitude of fault error + fault-free error + any unknown inherent bias with risk $\leq P_{LOIGF\_req}$. The only assumptions made are the fault-free errors in the broadcast ephemeris and clock and the errors in the IUM measurements are normally distributed with 0 mean and MS clock synchronization error = 0.

2.5 Least Squares Estimate

Recursive least squares [2, p 33-35] is selected as the algorithm for combining a sequence of multiple snapshot range measurements into an independent solution of SV ephemeris and clock error. The least squares algorithm is chosen because it is not based on past orbital history or model, thus providing a completely independent estimation. Snapshot estimates are given by

$$\mathbf{E}_0 = \left(\mathbf{H}_0^T \mathbf{W}_{meas,0} \mathbf{H}_0\right)^{-1} \mathbf{H}_0^T \mathbf{W}_{meas,0} \delta\mathbf{r}_0 \text{ (one snapshot)} \tag{22}$$

$$\mathbf{E}_{q+1} = \mathbf{E}_q + \mathbf{K}_{q+1}\left(\mathbf{r}_{q+1} - \mathbf{H}_{q+1}\mathbf{E}_q\right) \text{(multiple snapshots)} \tag{23}$$

E: estimate of the errors in the SV broadcast ephemeris and clock

q: update index

K: gain

$\delta\mathbf{r}$: range measurement error vector defined in (1)

H: measurement matrix for SV position and clock error solution

$\mathbf{W}_{meas}$: diagonal weight matrix representing the monitor receiver measurement errors (inverse of measurement error variances)

The covariance matrix (**cov**) of the SV ephemeris and clock error solution is given by

$$\mathbf{cov}_0 = \left(\mathbf{H}_0^T \mathbf{W}_{meas,0} \mathbf{H}_0\right)^{-1} \tag{24}$$

$$\mathbf{S}_{q+1} = \mathbf{H}_{q+1}\mathbf{cov}_q\mathbf{H}_{q+1}^T + \mathbf{W}_{meas,q+1}^{-1} \tag{25}$$

$$\mathbf{K}_{q+1} = \mathbf{cov}_q - \mathbf{H}_{q+1}^T\mathbf{S}_{q+1}^{-1} \tag{26}$$

$$\mathbf{cov}_{q+1} = \mathbf{cov}_q - \mathbf{K}_{q+1}\mathbf{S}_{q+1}\mathbf{K}_{q+1}^T \tag{27}$$

The above recursive least squares equations can be implemented in either ECEF or satellite HCLT coordinate frame. The algorithm is implemented in HCLT in the model used for analysis because it is more reasonable to assume that the errors to be estimated by the recursive least squares remain constant in HCLT frame rather than in the ECEF frame. The conversion of E, H and cov between ECEF and HCLT are

$$\mathbf{E}_{ECEF} = \mathbf{M}\mathbf{E}_{HCLT} \tag{28}$$

$$\mathbf{H}_{ECEF} = \mathbf{H}_{HCLT}\mathbf{M}^{T} \tag{29}$$

$$\mathbf{cov}_{ECEF} = \mathbf{M}\mathbf{cov}_{HCLT}\mathbf{M}^{T} \tag{30}$$

Where the mapping matrix **M** is a 4x4 matrix constructed as

$$\mathbf{M} = \begin{bmatrix} \mathbf{h}_{ECEF,3x1} & \mathbf{c}_{ECEF,3x1} & \mathbf{l}_{ECEF,3x1} & \mathbf{0}_{3x1} \\ 0 & 0 & 0 & 1 \end{bmatrix} \tag{31}$$

Where $\mathbf{h}_{ECEF,3x1}, \mathbf{c}_{ECEF,3x1}, \mathbf{l}_{ECEF,3x1}$ are the unit vectors of the axes of the satellite HCLT coordinate frame represented in ECEF coordinate frame.

2.6 Assumed $\mathbf{W}_{meas}$

$\mathbf{W}_{meas}$ is a parameter of (22), (24) and (25). Its diagonal elements are calculated as

$$W_{i,i\_meas}(el_i) = \left(\sigma^2_{cnmp}(el_i) + \sigma^2_{tropo}(el_i) + \sigma^2_{clock}\right)^{-1} \tag{32}$$

i: monitor station time and elevation angle index

σ_{cnmp}: standard deviation of errors due to monitor receiver code and multipath noise sources, a function of time (t_i) since acquisition

σ_{tropo}: standard deviation of errors due to un-modeled troposphere delay, a function of elevation angle (el_i) to the SV

σ_{clock}: standard deviation of monitor receiver clock synchronization error (monitor clocks are synchronized)

The equations for σ_{cnmp} and σ_{tropo} are defined in Appendix A. σ_{clock} is assumed = 0 for this performance analysis.

2.7 Measurement Process

The measurement process is a sliding window to account for pop-up fault induced errors at any time. The snapshot measurements of an SV are separated by $\Delta\tau$. $\Delta\tau$ is the minimum interval between independent measurements. $\Delta\tau$ is determined by the measurement error correlation time due to multipath and estimator smoothing. In this study it is assumed that $\Delta\tau$ = 5 min. The SV broadcast ephemeris and clock correction data are assumed to be updated by the OCX every 15 min. $\Delta\tau$ and the broadcast update interval constrain the number of estimation recursions. Figure 3 illustrates the measurement constraint. In the figure, each step indicates the maximum number of snapshots that would be available if the leading edge of the sliding window started at time (τ).

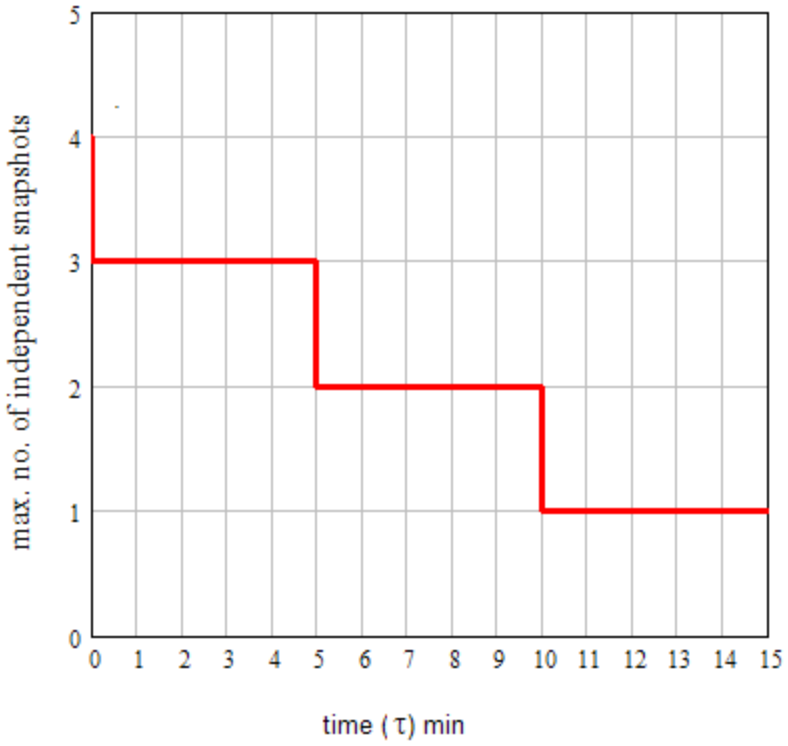

Figure 3 Graphical Illustration of Model Measurement Constraint

For monitoring URA prior to upload, four sets of snapshots could be processed during each 15 min interval between SV updates:

4 snapshots at $\tau = 0^+, 5, 10, 15^-$ min

3 snapshots at $\tau = 5, 10, 15^-$

2 snapshots at $\tau = 10, 15^-$

1 snapshot at $\tau = 15^-$

0^+: start time of new upload interval

15^-: maximum time to make URA decision

In practice to account for a fault-induced error occurring after 10 min, integrity credit with respect to monitoring URA may only be given for the one snapshot MMU at 15^- min. For example, assume that a fault error occurs after 10 min and is just above the threshold for a single snapshot decision. However, in the four snapshot decision at 15^- min (0^+, 5, 10 15^-) that same fault error would be diluted by ≅ 1/4 in the decision statistic while the threshold would be decreased by ≅ 1/2 so that the error might not be detected.

2.8 Monitor Error Characteristics

Figures 4 and 5 illustrate monitor error characteristics of four parameters using a SV / monitor stations geometry sample from an example GPS III constellation. These parameters are evaluated at locations in the SV footprint at a constant user elevation angle to the SV. The illustrated parameters are actual projected broadcast error, monitor estimate of that projected error, 5.73 MMU_{PL} bound and the monitor threshold. The first graph of each figure illustrates a simulated fault-free ephemeris error case. The other three figures illustrate assumed ephemeris fault-induced + simulated fault-free error cases. The fault cases assume 5 m biases in each of the SV HCL coordinates with variation of the sign of the biases.

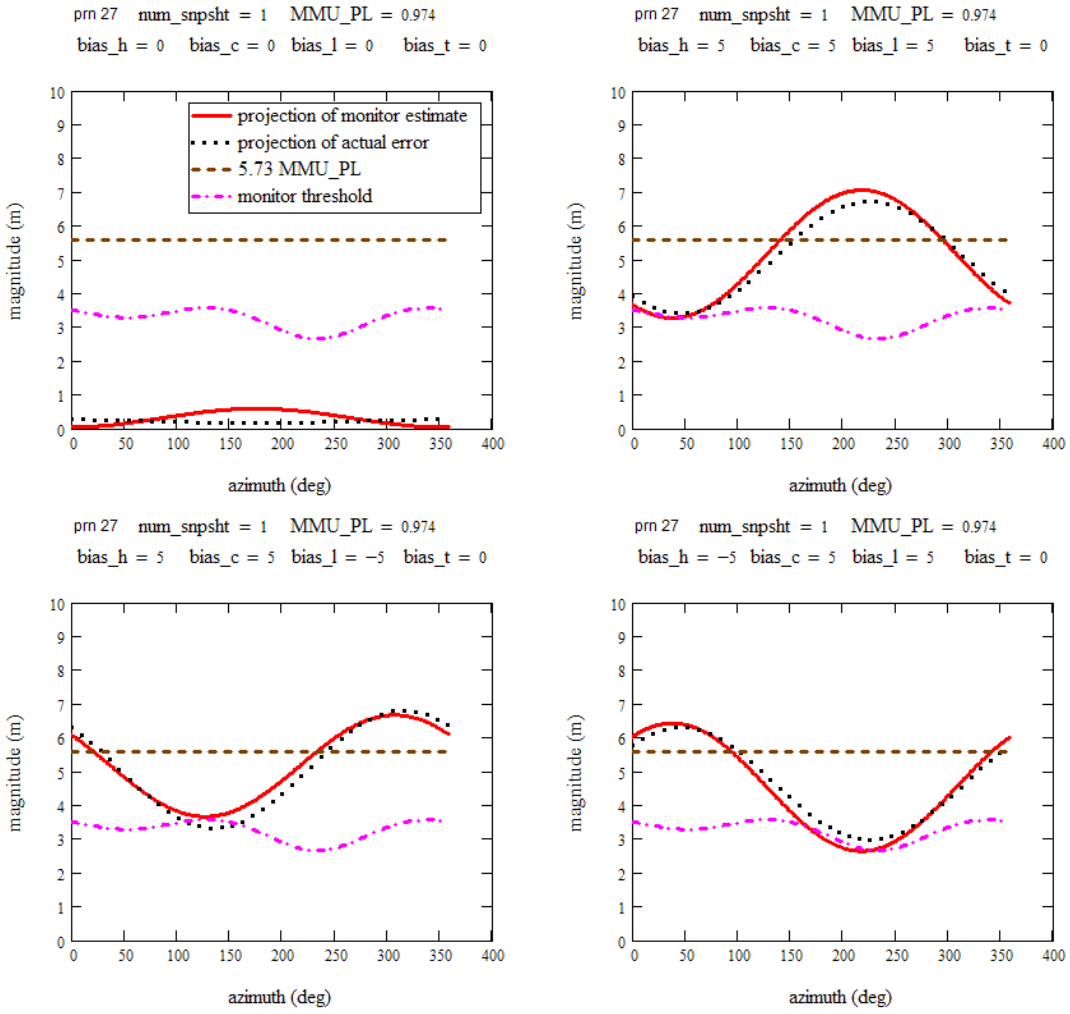

Figure 4 Example of Error Characteristics: One Snapshot

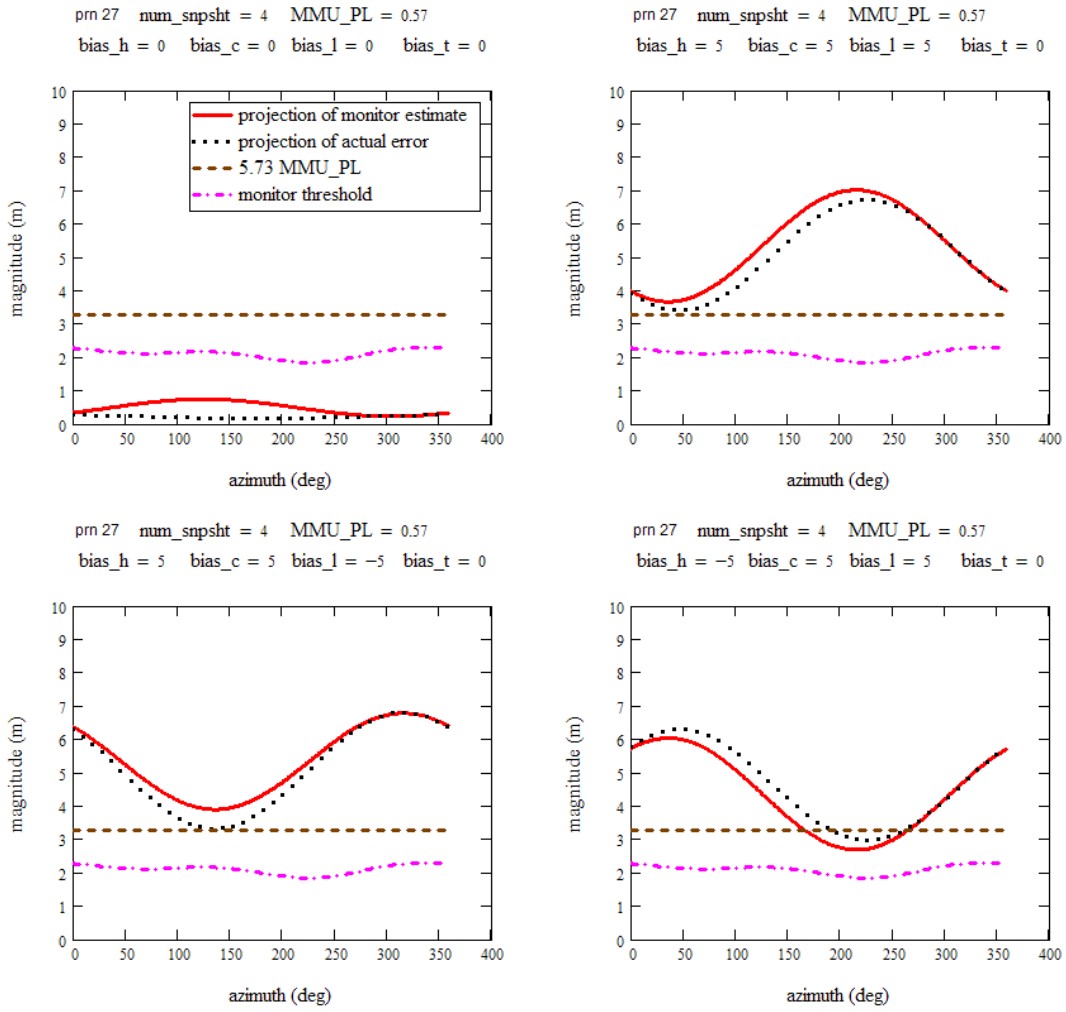

Figure 5 Example of Error Characteristics: Four Snapshots

Comparison of the figures indicates an approximate 40% reduction in MMU and mean threshold between 1 and 4 snapshots. Also, the phase of the actual error and its monitor estimate change as the sign of the SV ephemeris bias error components changes. Since the error phase is unpredictable, the maximum probability of missing the detection of a fault error would occur at the location of the peak threshold in the footprint.

3 IUM Performance Model

3.1 MMU_{PL} Parameters

The computation of MMU_{PL} requires four parameters (16). The threshold component requires three parameters (4): k_T, $\sigma_{i,\,k\_meas}$, and $\sigma_{i,\,k\_ure}$. The fourth parameter is K_{md}.

k_T

k_T sets the false detection probability. Since threshold comparisons at sample locations in the footprint are not independent, the derivation of k_T is complicated. For the performance model, upper and lower bounds on k_T are derived. The upper bound derivation assumes that all threshold decisions are independent. The lower bound derivation assumes that all threshold decisions are identical.

The upper bound of k_T (k_{T_ub}) is derived by assuming the false detection rate requirement is ≤ 1 / year per SV and the footprint location grid spacing is 1°. In spherical coordinates, the grid points are located at zenith angles 0, 1. . .76° and azimuth 0, 1…359°. Therefore, there are 77 × 360 = 27,720 grid points. Since the SV update occurs every 15 min, there are 4 URA decisions / h. Therefore, the upper bound probability of false detection (P_{fd_ub}) is

$$P_{fd\_ub} = (365 \times 24 \times 4 \times 27{,}720)^{-1} = 1.03 \times 10^{-9} \text{ with corresponding } k_{T\_ub} = 6.11 \qquad (33)$$

The 1° grid spacing is chosen to capture an accurate maximum threshold and to be conservative (authors' opinion). If the false detection probability were derived exactly, the correlation between grid points would have to be accounted for.

The lower bound of k_T (k_{T_lb}) is

$$P_{fd\_lb} = (365 \times 24 \times 4 \times 1)^{-1} = 2.854 \times 10^{-5} \text{ with corresponding } k_{T\_lb} = 4.19 \qquad (34)$$

To investigate the difference in threshold multipliers, a simulation of 100 random SV/MS geometries was run to compare the one snapshot MMU_{PL} computed from the two values of k_T. The results are presented in Figure 6, where it is shown that there is a near constant 25% difference in magnitudes, min{ratio} = 1.243, max{ratio} = 1.251. The subsequent performance analysis assumes k_T = 6.11, which produces the larger MMU.

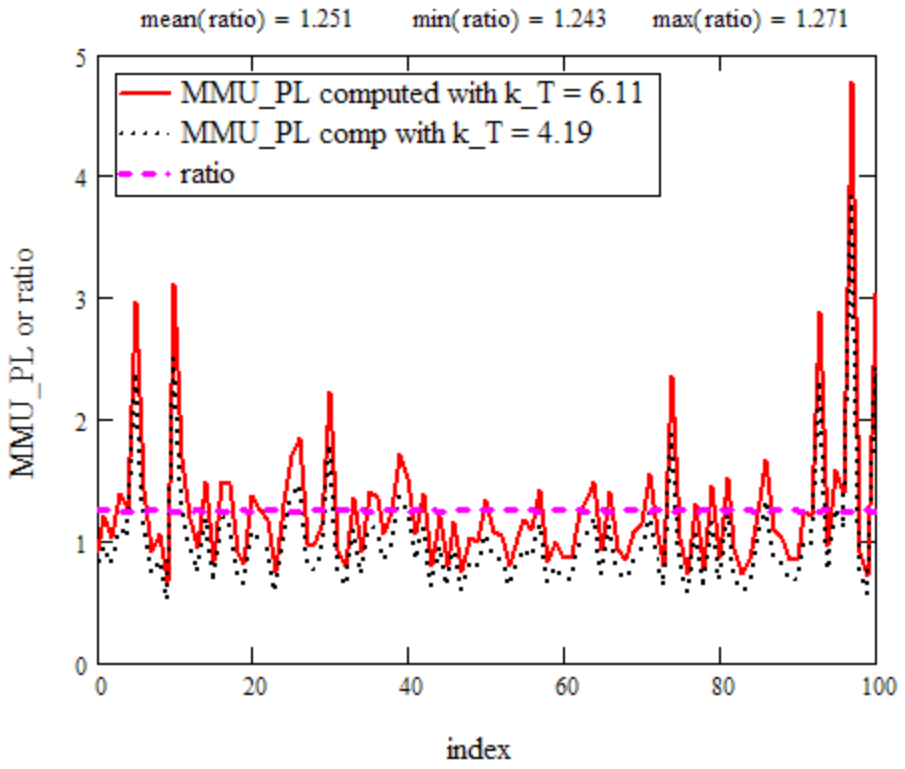

Figure 6 Effect of Threshold Multiplier (k_T) on Magnitude of MMU_{PL}

$\sigma_{i,\ k\_meas}$

Referring to (30)

$$\sigma_{i,\,k\_meas} = \sqrt{\mathbf{L}_{i,\,k}^{T}\ \mathbf{cov}_{HCLT}\ \mathbf{L}_{i,\,k}} \tag{35}$$

$\sigma_{i,\ k\_ure}$

An assumed covariance matrix of the fault-free errors in the ephemeris and clock correction broadcast ($\mathbf{C}_{ure}$) is needed to calculate σ_{ure}. An analysis of actual GPS data was performed in order to assemble a typical covariance ($\mathbf{C}_{typ}$) that is based on broadcast ephemeris and clock correction data and precise ephemeris and clock correction data from a present GPS SV. The data for formulating $\mathbf{C}_{typ}$ was processed from data obtained from the NGA website for a typical SV, as described in Appendix B.

$$\mathbf{C}_{typ} = \begin{bmatrix} 0.0608 & -0.0104 & -0.0820 & 0.2724 \\ -0.0104 & 0.2216 & -0.2415 & -0.0495 \\ -0.0820 & -0.2415 & 0.9456 & -0.4499 \\ 0.2724 & -0.0495 & -0.4499 & 1.5495 \end{bmatrix} \text{ in HCLT coordinates} \tag{36}$$

A GPS IIIC era ephemeris and clock RMS error over the SV footprint is assumed to be σ_{ure} = 0.25 m. Using an equation derived in [3, p 598], this RMS value is satisfied by finding a multiplier, a, such that

$$\sigma_{ure} = a\sqrt{\frac{1}{49}\left[C_{typ\_2,2} + C_{typ\_3,3} + 0.959\left(C_{typ\_1,1} + C_{typ\_1,4} + 1.959\,C_{typ\_4,4}\right)\right]} = 0.25\,\text{m} \quad (37)$$

$$a = 0.1699 \quad (38)$$

The assumed $\mathbf{C}_{ure} = a^2\,\mathbf{C}_{typ}$

$$\mathbf{C}_{ure} = \begin{bmatrix} 0.1754 & -0.0299 & -0.2366 & 0.7864 \\ -0.0299 & 0.6395 & -0.6972 & -0.1428 \\ -0.2366 & -0.6972 & 2.7295 & -1.2986 \\ 0.7864 & -0.1428 & -1.2986 & 4.4725 \end{bmatrix} \times 10^{-2} \quad (39)$$

$$\sigma_{i,k\_ure} = \sqrt{\mathbf{L}_{i,k}^{T}\,\mathbf{C}_{ure}\,\mathbf{L}_{i,k}} \quad (40)$$

K_{md}

K_{md} is contained and defined in the MMU_{PL} equations (15 - 17). Assuming $P_{md} = 10^{-4}$ and using typical values for the other parameters, K_{md} = 3.72.

3.2 Summary of Performance Model Parameters

Table 1 contains a summary of the assumed parameters of the performance model and their temporal behavior.

Table 1 Performance Model Parameters

Parameter	Temporal Behavior
SV broadcast fault-induced error	Constant during an estimation window
SV broadcast fault-free error	Normal distribution, constant during an estimation window
Monitor receiver code noise, multipath error (CNMP)	Normal distribution, variable at each independent snapshot, error is function of time since acquisition of SV signal
Troposphere delay	Normal distribution, variable at each independent snapshot, error is a function of elevation angle
Measurement matrix (**H**)	Based on a model of GPS III Nominal 27/6 Constellation, function of time, and satellite and monitor receiver locations

4 MMU Results

This section summarizes the MMU results obtained from the performance model for one snapshot and four snapshots. The analysis relies on the same network of 17 MSs currently used by the GPS control segment.

4.1 Assumed Monitor Receiver Elevation Angle Mask

To illustrate IUM global coverage sensitivity to the selection of elevation mask angle, global MMU results assuming 10° mask angle for USAF and 15° mask angle for NGA monitor stations are first presented. Thereafter, the selected mask angle for the IUM is 5°, the value used in the FAA's Wide Area Augmentation System (WAAS).

4.2 Worldwide MMU results

Figures 7 and 8 contain graphical overviews of worldwide MMU values assuming 10°, 15° IUM elevation angle masks and 5° IUM elevation angle masks, respectively. Note in Figure 7 and 8 the dots correspond to a 5 min time step. Based on the data of Figure 7, the percent of unmonitored SVs is 22.6% for the assumed 10°, 15° elevation angle masks. The unmonitored results are indicated by the white gaps in the SV traces. Unmonitored SV means that less than 4 MS view the SV. Referring to Figure 8, the percent of unmonitored SVs obtained assuming a 5° elevation mask angle is 2.8%.

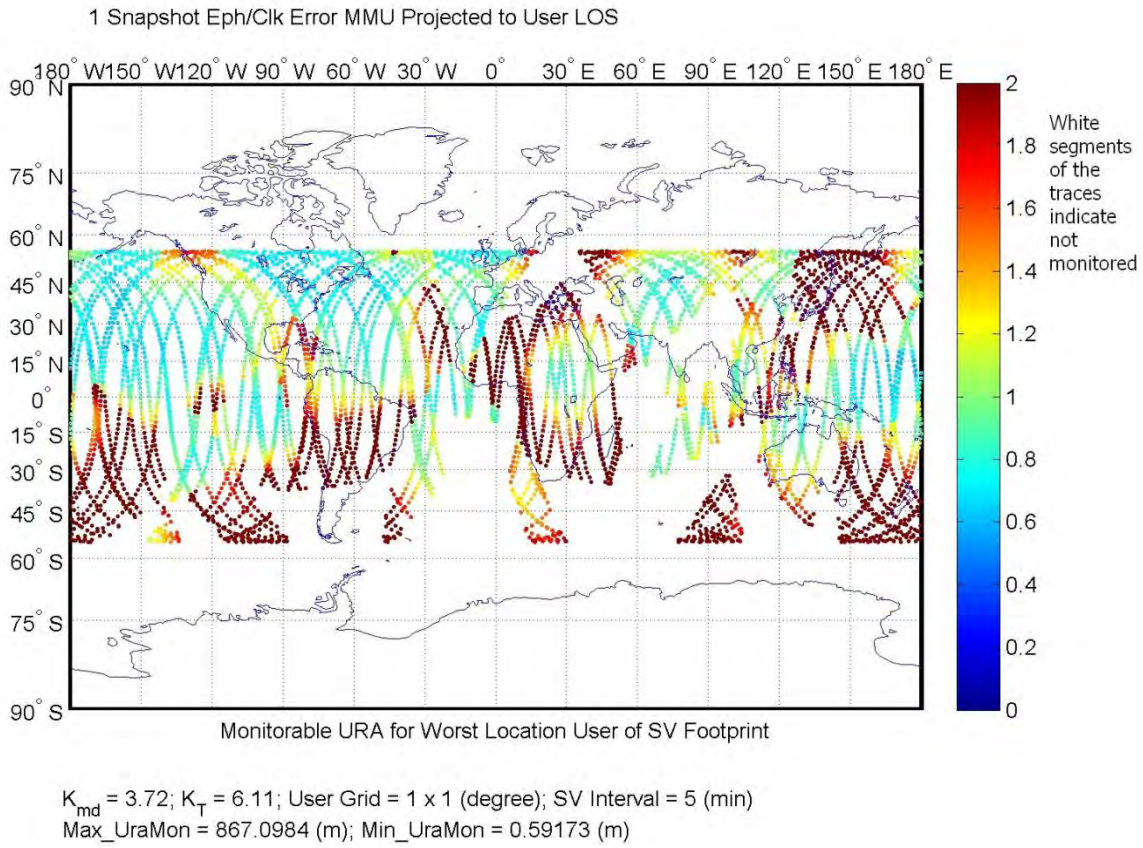

Figure 7 GPS III SV Ground Tracks with MMU Magnitude in Color Code: One Snapshot, Monitor Receiver Elevation Mask Angle = 10^0 (USAF), 15^0 (NGA)

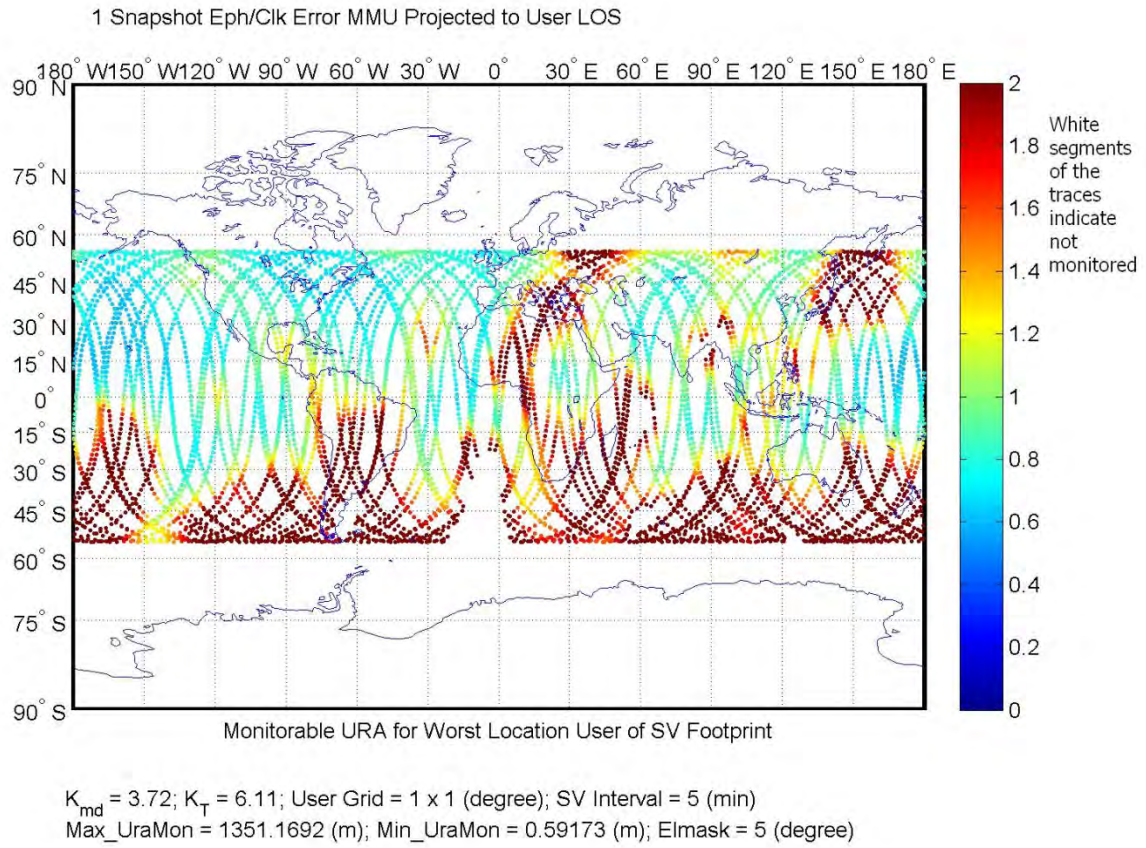

Figure 8 GPS III SV Ground Tracks with MMU Magnitude in Color Code: One Snapshot, Monitor Receiver Elevation Mask Angle = 5^0

Figure 9 contains the worldwide MMU results for four snapshots and 5° IUM mask angle. In Figure 9 the dots correspond to a 15 min time step. Table 2 compares worldwide percentiles for one snapshot and four snapshot MMUs. Compared to one snapshot, four snapshots would yield significantly smaller values of MMU.

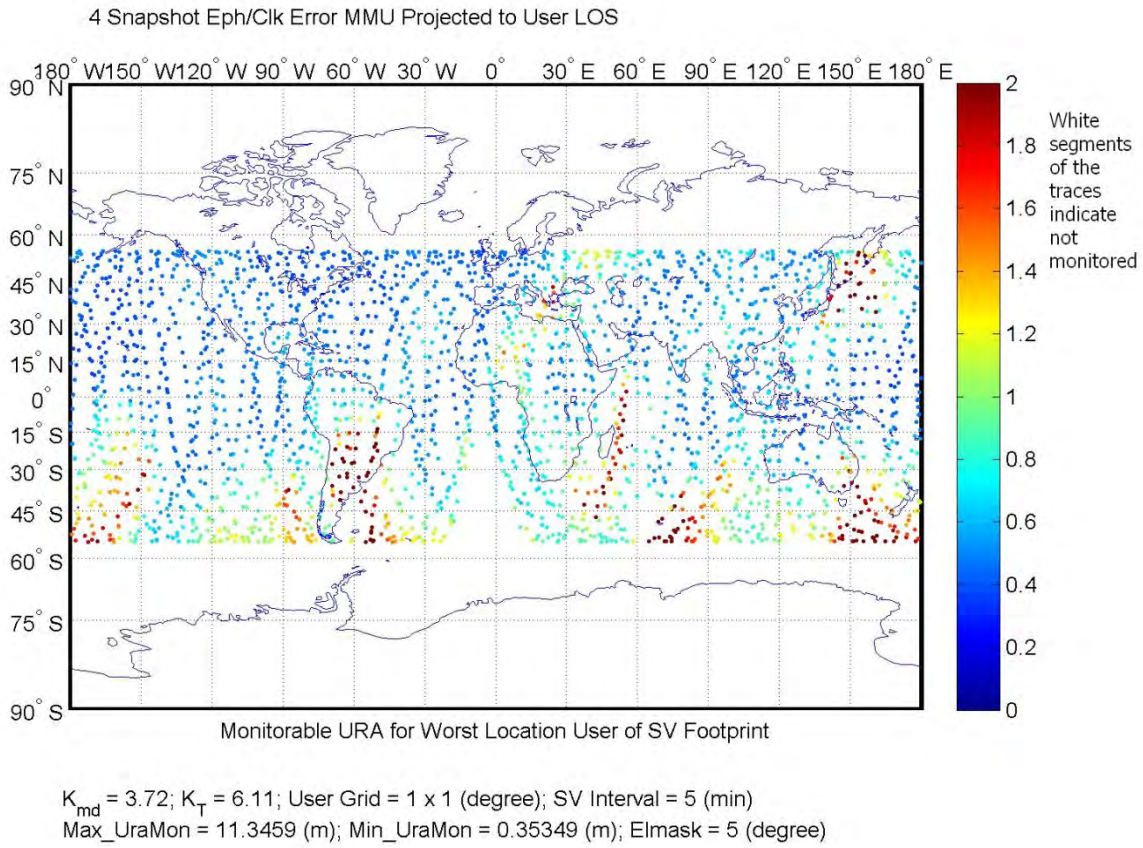

Figure 9 GPS III SV Ground Tracks with MMU Magnitude in Color Code: Four Snapshots, Monitor Receiver Elevation Mask Angle = 5^0

Table 2 Worldwide MMU Percentiles

%-tile	1 snapshot (m)	4 snapshots (m)
0	0.59	0.35
20	0.82	0.45
30	0.90	0.49
40	1.01	0.54
50	1.17	0.61
60	1.41	0.70
70	1.77	0.85
80	2.21	1.04
90	3.14	1.42
95	4.36	1.85
maximum	1351	11.3

4.3 MMU Results at Specific Locations

4.3.1 U. S. Locations

One snapshot MMU percentiles at eight U.S. city locations (locations of major airports) are displayed in Table 3. For these locations MMU values beyond the 20%-tile, are greater than the desired value of integrity assured URA ≤ 0.7 m for GPS IIIC. Median values are approximately 0.8 – 0.9 m.

Table 3 U.S. Location: MMU Computed From One Snapshot

%-tile and other statistics	Seattle (m)	San Diego (m)	Minn./ St. Paul (m)	Houston (m)	Boston (m)	Miami (m)	Juneau (m)	Honolulu (m)
0 %	0.592	0.592	0.601	0.601	0.601	0.601	0592	0.592
20	0.710	0.711	0.721	0.722	0.733	0.731	0.714	0.715
40	0.792	0.799	0.803	0.802	0.817	0.810	0.807	0.828
50	0.831	0.845	0.844	0.840	0.865	0.852	0.861	0.898
60	0.887	0.899	0.895	0.896	0.920	0.907	0.918	0.982
80	1.079	1.150	1.070	1.089	1.166	1.122	1.137	1.523
90	1.435	1.560	1.338	1.417	1.609	1.652	1.569	2.354
95	2.304	2.200	1.917	1.980	2.544	3.043	2.501	3.290
99	14.626	13.462	3.909	9.865	5.942	28.482	13.871	14.626
maxi-mum	867.1	867.1	8.928	38.625	21.824	1351	867.1	867.1
% un-mon	0	0	0	0	0	0.241	0	0
no. of samples	2523	2507	2489	2487	2457	2483	2718	2531

4.3.2 Non-U.S. Locations

MMU percentiles based on one snapshot at ten non-U.S. locations are displayed in Table 4. The MMUs are larger than those for the U.S. The median values are approximately 0.9 – 1.5 m. For these locations MMU values beyond the 0%-tile are greater than the desired value of integrity assured URA ≤ 0.7 m for GPS IIIC.

Table 4 Non-U.S. Locations: MMU Computed from One Snapshot

%-tile and other statis-tics	London (m)	Frank-furt (m)	Mos-cow (m)	Beij-ing (m)	Tokyo (m)	Rio de Jan-eiro (m)	Buenos Aires (m)	Cape Town (m)	Sydney (m)	Welling-ton (m)
0 %	0.639	0.639	0.639	0.592	0.592	0.639	0.650	0.654	0.592	0.592
20	0.786	0.786	0.801	0.796	0.759	0.872	0.919	1.048	0.897	0.876
40	0.884	0.887	0.925	0.944	0.905	1.166	1.206	1.513	1.256	1.358
50	0.942	0.954	1.004	1.023	0.984	1.378	1.384	1.732	1.516	1.733
60	1.014	1.034	1.101	1.119	1.066	1.659	1.635	1.952	1.872	1.984
80	1.317	1.373	1.529	1.444	1.384	2.276	2.246	2.882	2.704	2.824
90	1.677	1.802	2.212	2.111	1.924	3.026	2.848	4.268	3.723	3.750
95	2.245	2.350	3.233	3.075	2.948	4.296	4.268	6.971	5.248	5.099
99	3.579	4.023	12.795	14.710	14.710	28.482	31.462	31.462	10.004	9.839
maxi-mum	5.501	8.928	33.289	867.1	867.1	1351	1351	1351	867.1	23.000
% un-moni-tored	0.12	0.764	1.053	0.976	0.565	5.985	6.209	7.957	1.276	5.67
no. of sam-ples	2506	2469	2630	2435	2467	2419	2296	2244	2476	2457

4.4 Comparison of One and Four Snapshot Derived MMUs

Table 5 contains a comparison between median MMU values based on one snapshot and four snapshots. There is an approximate 50% reduction in MMU magnitude when four snapshots are used. An MMU based on four snapshots is more likely to meet the desired URA $\leq$ 0.7 m. However, as noted previously, multi-snapshot estimates may not detect a fault error occurring toward the end of a recursion interval so that only a one snapshot MMU may be acceptable.

Table 5 Comparison of Median Values of MMUs Based on One and Four Snapshots

Location	Median MMU_PL 1 snapshot (m)	Median MMU_PL 4 snapshots (m)	Ratio MMU_PL(4 snap.) / MMU_PL(1 snap.)
Seattle	0.831	0.460	0.554
San Diego	0.845	0.467	0.553
Minn. / St. Paul	0.844	0.465	0.551
Houston	0.840	0.465	0.554
Boston	0.865	0.475	0.549
Miami	0.852	0.467	0.548
Juneau	0.861	0.473	0.549
London	0.942	0.508	0.539
Frankfort	0.954	0.514	0.539
Moscow	1.004	0.532	0.530
Beijing	1.023	0.545	0.533
Tokyo	0.984	0.529	0.538
Rio de Janeiro	1.378	0.688	0.499
Buenos Aires	1.384	0.693	0.501
Cape Town	1.732	0.839	0.484
Sydney	1.516	0.743	0.490
Wellington	1.733	0.827	0.477

4.5 MMU Variation

MMU varies over time with SV motion. The variation depends upon the number of monitor stations that can observe the SV above the elevation mask angle and the geometry of the error projection onto the location with the maximum monitor threshold (T_{max}). Figure 10 contains example variations over 24 h for MMUs based on one and four snapshots. When MMU is based

on four snapshots, the large peak variations are significantly suppressed. This suppression is usually due to an increase in the number of monitor stations viewing the SV within the 4 snapshot window. The range of typical ratios of MMU derived from four snapshots to those derived from one snapshot is 0.4 – 0.6. During periods of extremely poor geometry even smaller ratios occur (e.g., 0.21).

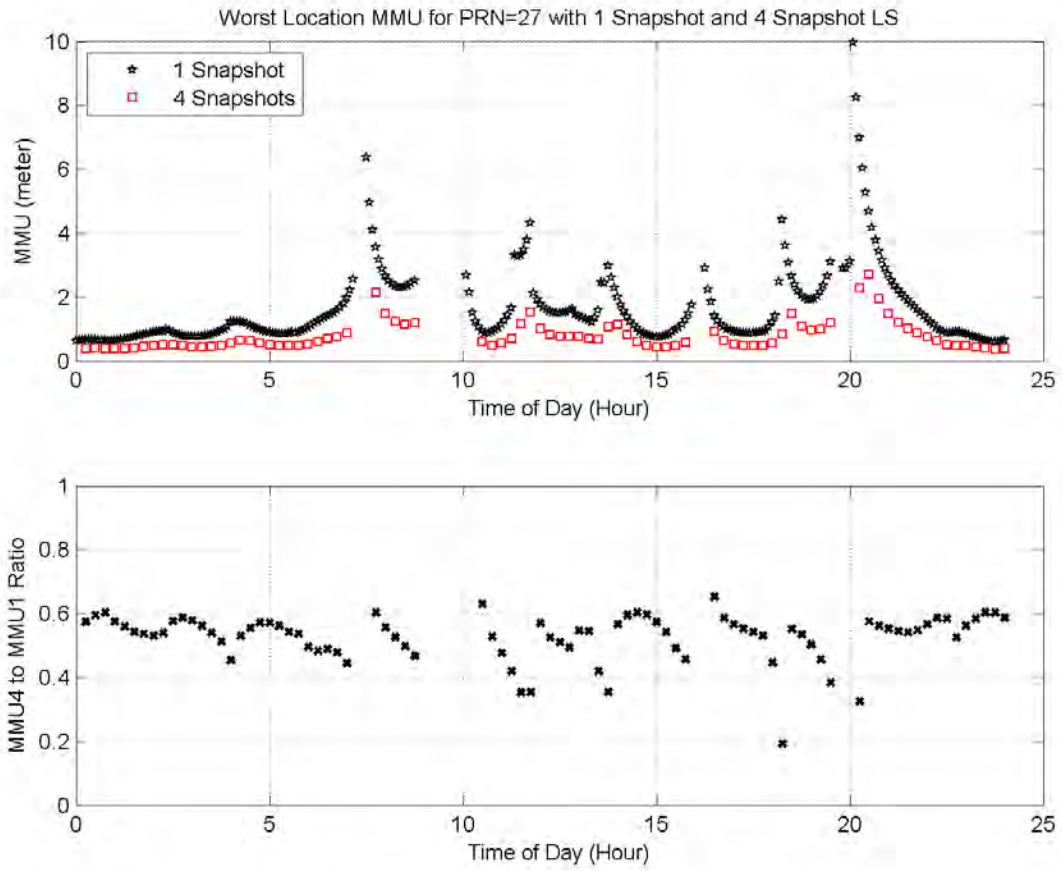

Figure 10 Example MMU Variation Versus Time Along SV Track

5 Application to LPV200

5.1 User Error Model

5.1.1 Error Equations

In addition to an MMU serving to bound SIS errors, the LPV200 application requires an airborne user receiver error model since the navigation sensor error (NSE) includes both SIS and user receiver measurement errors. The user based errors are assumed to be due to receiver noise, multipath noise and residual troposphere error, characterized by σ_{rn}, σ_{mp} and σ_{tropo}, respectively. The standard deviation equations are from [4] for single frequency errors.

$$\sigma_{mp}(el_j) = 0.13 + 0.53 \exp\left(\frac{-el_j}{10}\right) \text{ m (multipath)} \tag{41}$$

$$\sigma_{rn} = 0.15 \text{ m (receiver noise sigma for accuracy designator B at min signal level)} \tag{42}$$

$$\sigma_{tropo}(el_j) = 0.12 \frac{1.001}{\sqrt{0.002001 + \sin^2(el_j)}} \text{ m} \tag{43}$$

j: SV index

el: elevation angle to SV in deg

The total user dual-frequency range measurement error standard deviation for SV_j is

$$\sigma_{tot}(el_j) = \sqrt{MMU_j^2 + \sigma_{rnmp}^2(el_j) + \sigma_{tropo}^2(el_j)} \tag{44}$$

$$\sigma_{rnmp}^2(el_j) = d^2\left[\sigma_{mp}^2(el_j) + \sigma_{rn}^2\right] \tag{45}$$

d: dual-frequency error multiplication factor = 2.59

The diagonal elements of the user position solution integrity weight matrix ($\mathbf{W}_I$) are given by

$$W_{j,j\_I} = \sigma_{tot}^{-2}(el_j) \tag{46}$$

The user position solution limits are assumed to be elevation angle ≥ 5° and MMU ≤ 10 m.

5.1.2 Over Bound

The vertical requirements for LPV200 are significantly more difficult to achieve than the horizontal requirements. Therefore, their achievement usually also implies achievement of horizontal requirements. All of the LPV200 application results are based on the root-sum-square (RSS) of the projections of the $\sigma_{tot}(el_j)$ onto the user's vertical position direction.

$$\sigma_{vert} = \sqrt{\sum_{j=1}^{N} S_{3,j}^2 \, \sigma_{tot}^2(el_j)} \tag{47}$$

$S_{3,j}$: solution vertical projection coefficient for SV_j

N: number of SVs in solution

For σ_{vert} to be used in satisfying the integrity of the position solution, each $\sigma_{tot}(el_j)$ has to be the standard deviation that characterizes a normal distribution, $N\{0, \sigma^2_{tot}(el_j)\}$, that over bounds the distribution of the user's total range error for each SV_j, as proven in [5]. Based on an analysis in [6], Appendix C contains a definition and analysis of an over bounding concept where multiples of MMU are the bounds on the SIS component of the total user range error. The appendix illustrates that over bounding is achieved for the SIS errors for this application when $P_{fault} \leq 10^{-4}$ / h, $P_{LOIGF\_req} = P_{alloc} / P_{fault} = 10^{-8} / P_{fault}$. The remaining components of the total range error distribution are conventionally assumed to be over bounded by $N\{0, \sqrt{\sigma^2_{rnnp} + \sigma^2_{tropo}}\}$ (44 – 45).

5.2 LPV200 Requirements

There are four NSE vertical requirements that need to be satisfied for LPV200 as identified in [6]. It is noted that there is also a 6 s integrity response time that is not addressed by the IUM since the OCX updates are every 15 min. The 6 s response time would conceptually be addressed by an on-board SV monitor. The four requirements are presented below.

5.2.1 Fault-Present Vertical Requirements

- Vertical protection level (VPL) ≤ 35 m
- $Prob\{NSE|_{fault\ present} \leq 15\ m\} \geq 1 - 10^{-5}$

5.2.2 Fault-Free Vertical Requirements

- $Prob\{NSE|_{fault\ free} \leq 4\ m\} \geq 0.95$
- $Prob\{NSE|_{fault\ free} \leq 10\ m\} \geq 1 - 10^{-7}$

5.3 Performance Measure

Availability of service is a standard performance measure when assessing the operational feasibility of an integrity concept. The availability models that are described assume that the full constellation of 27 SVs is in operation (no SV outages). A more rigorous availability model would account for SV outages. Therefore, the availability results are slightly optimistic.

5.3.1 Vertical Protection Level (VPL) Availability

$$\mathbf{C}_I = \left(\mathbf{H}^T_{user}\, \mathbf{W}_I \mathbf{H}_{user}\right)^{-1} \tag{48}$$

$$VPL = K_{VPL} \sqrt{\left(\mathbf{C}_I\right)_{3,3}} \tag{49}$$

$\mathbf{H}_{user}$: user measurement matrix

$\mathbf{C}_I$: covariance matrix with integrity weight $\mathbf{W}_I$

$$\sqrt{C_{I\,3,3}} = \sigma_{vert} \tag{50}$$

K_{VPL}: VPL multiplier = 5.33 (corresponds to WAAS LPV200)

$$avail_{VPL} = \frac{no.(VPL \le 35\,m)}{N} \tag{51}$$

N: no. of samples = 288 per location (sampling interval = 5 min over 24 h)

5.3.2 NSE Fault-Present Availability

$$NSE|_{fault\ present} = 4.42\sqrt{C_{I\,3,3}} \quad (4.42 \text{ corresponds to probability} = 1 - 10^{-5}) \tag{52}$$

$$avail_{fault\ present} = \frac{no.(NSE|_{fault\ present} \le 15\,m)}{N} \tag{53}$$

5.3.3 NSE Fault-Free Availability

The position solution uses integrity weight matrix $\mathbf{W}_I$ that is based on MMU, but the fault-free component in the total range error variance has to be represented by σ^2_{ure} rather than MMU. Define

$$W_{j,j\_ff} = \left(\sigma^2_{ure} + \sigma^2_{rmnp}(el_i) + \sigma^2_{tropo}(el_i)\right)^{-1} \tag{54}$$

$$\sigma_{ure} = 0.3\ m \tag{55}$$

$$\mathbf{S} = (\mathbf{H}^T\,\mathbf{W}_I\,\mathbf{H})^{-1}\,\mathbf{H}^T\,\mathbf{W}_I \tag{56}$$

The fault-free error covariance is

$$\mathbf{C}_{ff} = \mathbf{S}\,\mathbf{W}_{ff}^{-1}\,\mathbf{S}^T \tag{57}$$

$$avail_{ff}(K_{ff}, V) = \frac{no.(K_{ff}\sqrt{C_{ff\,3,3}} \le V)}{N} \tag{58}$$

$$avail_{fault\ free}|_{NSE \le 4\,m} = avail_{ff}(1.96, 4\,m) \quad (1.96 \text{ corresponds to prob.} = 0.95) \tag{59}$$

$$avail_{fault\ free}|_{NSE \le 10\,m} = avail_{ff}(5.33, 10\,m) \quad (5.33 \text{ corresponds to prob.} = 1 - 10^{-7}) \tag{60}$$

The achieved availability is the fraction of the number of time steps (N_{sat}) where all four availability requirements are satisfied

$$avail_{achiev} = \frac{N_{sat}}{288} \tag{61}$$

5.4 Availability Results

5.4.1 U.S. Locations

Availability results for the sample U.S. locations are contained in Table 6. As stated previously the availability values are based on no SV outages. It is seen that most achieved availabilities are 1 and the lowest availability (0.993) occurs at Houston and Juneau.

Table 6 Availability at U.S. Locations (No SV outages and All-In-View, One Snapshot MMU)

location	avail fault error VPL ≤ 35 m	avail fault present NSE ≤ 15 m	avail fault free NSE ≤ 4 m	avail fault free NSE ≤10 m	achieved availability
Seattle	1	1	1	1	1
San Diego	1	1	1	0.997	0.997
Minneapolis St. Paul	1	1	1	1	1
Houston	1	1	1	0.993	0.993
Boston	1	1	1	1	1
Miami	1	1	1	1	1
Juneau	1	1	0.997	0.993	0.993
Honolulu	1	1	1	1	1

5.4.2 Non-U.S. Locations

Availability results for the sample non-U.S. locations are contained in Table 7. Except for London, Frankfort and Beijing, the availability results are ≤ 0.983. It is noted that it is desirable to achieve availability greater than 0.99 for LPV200 operation.

Table 7 Availability at non-U.S. Locations (No SV Outages, All-In-View, One Snapshot MMU)

location	avail fault error VPL ≤ 35 m	avail fault present NSE ≤ 15 m	avail fault free NSE ≤ 4 m	avail fault free NSE ≤10 m	achieved availability
London	1	1	1	1	1
Frankfort	1	1	1	1	1
Moscow	1	0.993	0.997	0.983	0.983
Beijing	1	1	1	1	1
Tokyo	1	0.990	0.986	0.962	0.962
Rio de Janeiro	1	0.872	0.941	0.899	0.847
Buenos Aires	0.976	0.688	0.851	0.802	0.663
Cape Town	0.972	0.656	0.924	0.858	0.622
Sydney	0.997	0.733	0.976	0.917	0.715
Wellington	0.986	0.674	0.958	0.938	0.670
North Pole	1	0.990	0.972	0.927	0.927
South Pole	0.934	0.215	0.705	0.521	0.170

5.4.3 Impact of Integrity Weight (W_I) on Solution Availability

Since $\mathbf{W}_I$ contains MMU, the position solution accuracy is degraded relative to the conventional least-squares solution that assumes fault-free performance. To gauge the loss of accuracy, fault-free vertical position availability using W_I and W_{ff} (least-squares weight) as solution weights are compared in Table 8. From Table 8, it is seen that there is no change in availability for the U.S. locations. However, the use of W_I at locations where there is poor geometry can adversely affect accuracy availability, as illustrated by the results for Rio de Janeiro and South Pole.

Table 8 Comparison of Fault-Free Availabilities Obtained From Position Solutions Using W_I and W_{ff} as Weight Matrices (No SV Outages, All-In-View, One Snapshot MMU)

location	avail NSE≤ 4 m solution weight = W_I	avail NSE≤ 4 m solution weight = W_{ff}	avail NSE≤ 10 m solution weight =W_I	avail NSE≤ 10 m solution weight = W_{ff}
Seattle	1	1	1	1
San Diego	1	1	0.997	0.997
Minneapolis St. Paul	1	1	1	1
Houston	1	1	0.993	0.993
Boston	1	1	1	1
Miami	1	1	1	1
Juneau	0.997	0.997	0.993	0.993
Rio de Janeiro	0.941	0.969	0.899	0.958
South Pole	0.705	0.958	0.521	0.910

6 Results Based on Assumptions and Analysis of Independent URA Monitor (IUM)

1. Based on SV position and clock error independently derived using measurements from receivers located at GPS monitor stations, ephemeris and clock integrity can be assured by an IUM prior to data upload to an SV.

2. The monitor receiver elevation mask angle should be no greater than 5° for effective coverage for independent SV position determination.

3. If the broadcast URA ≥ minimum monitorable URA (MMU) as defined in this paper, the GPS IIIC SV signal-in-space 5.73 URA error bound for $\leq 10^{-8}$ integrity risk would be assured for any ephemeris and clock error type (fault-free or fault-induced), provided that the SV fault error rate $\leq 10^{-4}$ / h.

4. For U.S. locations, the median and 95%-tile MMU values are approximately 0.8 – 0.9 m and 2 – 3 m, respectively (given the assumptions of the analysis).

5. For the non-U.S. locations considered, the median and 95% MMU values are approximately 0.9 – 1.7 m and 2 – 7 m, respectively (given the assumptions of the analysis).

6. The MMU values are generally greater than the GPS IIIC maximum specified URA broadcast value (0.7 m) (given the assumptions of the analysis). Therefore, if IUM were part of the OCX for GPS IIIC then the broadcast URA would usually be > 0.7 m.

7. The main limitations of the IUM as presented in this paper are:
    - IUM SV position determination is based on one snapshot. If SV position accuracy were enhanced by multiple snapshots, smaller values of MMU could be achieved. However, it would be more difficult to detect a fault error that occurred after the start of a measurement window since the fault error would be diluted to a greater extent than the threshold was lowered.
    - Since only one integrity parameter (URA) is broadcast, MMU has to be the peak value over the SV footprint in order to assure integrity at the worst user location in the SV footprint.
    - To simplify the performance analysis, it was assumed that the decision statistic errors at the monitor sample points in an SV footprint are independent. This assumption causes unnecessarily large monitor thresholds, which causes MMU to be greater than it would be if correlation between decision statistic errors were taken into account. Assuming maximum correlation would allow the MMU values to be reduced by 25% to their lower-bound values, the corresponding U.S. median and 95%-tile URA values would be approximately 0.6 m and 1.5 – 2.3 m,

respectively. Therefore, the URA ≤ 0.7 m requirement would still not be met in general.

8. Although IUM would not support a broadcast URA ≤ 0.7 m, it would still provide high availability for the stringent requirements of LPV200 approaches at U.S. airports. For all U.S. major airports considered, achieved availability ≥ 0.997 except for Houston and Juneau (0.993). However, LPV200 availability at the ten non-U.S. airports considered for analysis ranged between 0.6 – 1, with the degraded availability being most prominent in the southern hemisphere.

7 List of References

1 Kovach, K., J. Dobyne, M. Crews and C. Miles, *GPS III Integrity Concept*, Proceedings of ION GNSS 2008 (p 2250 – 2257), Sept. 2008.

2 Bar-Sholom, Y., Fortmann, T.E., *Tracking and Data Asso*ciation, Academic Press, 1988.

3 Zuberge, J. F. and Bertiger, W.I., *Ephemeris and Clock Navigation Message Accuracy, Global Positioning System: Theory and Applications*, Vol. 1, AIAA, 1996.

4 RTCA SC-159, *Minimum Operational Performance Standards for Global Positioning System / Wide Area Augmentation System Airborne Equipment*, RTCA DO-229D, December 13, 2006.

5 DeCleene, B., *Defining Pseudorange Integrity Over Bounding*, Proceedings of ION GPS 2000 (p 1916 – 1924), September 2000.

6 Shively, C., *Analysis of Specified and Hypothetical GPS IIIC Integrity for LPV200 Operati*ons, Proceedings of ION 2010 International Technical Meeting, January 2010.

7 MS receiver accuracy model is based on Shallberg, K. and Ericson, S. (private communication), *CNMP Considerations for Future Ground Stations*, GREI / Zeta Associates report, 6/12/2007.

Appendix A MS Receiver Error

The MS receiver errors are characterized by an error equation derived from the testing of an advanced monitor receiver [7]. The error equation models code noise and multipath noise (CNMP) as function of time (t) since an SV was acquired by the receiver.

$$\sigma_{CNMP} = \frac{Mean\_Error(t)}{K_{CNMP}} + \sigma_{carrier} \quad m \tag{A-1}$$

$$\begin{aligned} Mean\_Error(t) &= \max\left\{u \sin\left(2\pi \frac{t}{TL1}\right), FLOOR\right\}, \quad t < TL1/4 \\ &= \max\{1, FLOOR\}, \quad t > TL1/4 \end{aligned} \tag{A-2}$$

$$\begin{aligned} u &= \frac{A_0}{2\pi} \frac{TL1}{t}, \quad TL1 = 1600 \text{ s}, \quad A_0 = 10 \text{ m}, \quad FLOOR = 0.4 \text{ m}, \\ \sigma_{carrier} &= 0.03 \text{ m}, \quad K_{CNMP} = 3.29 \end{aligned} \tag{A-3}$$

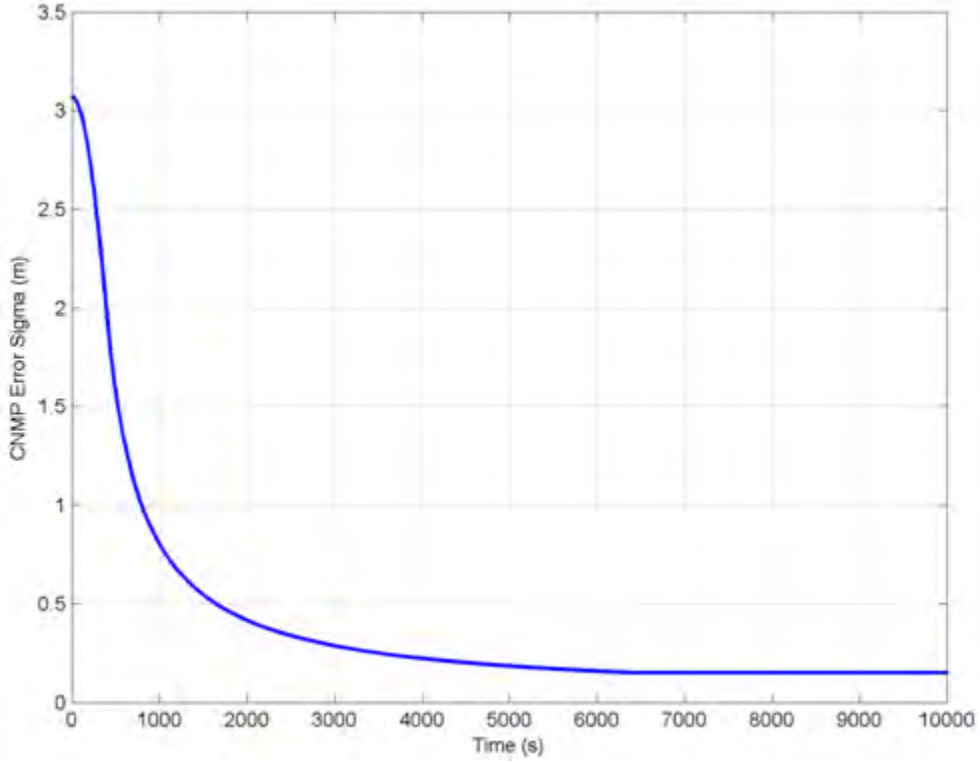

Figure 11 Monitor Receiver CNMP Error Standard Deviation

A.1 Residual Troposphere Error

The MS error due to residual troposphere delay error is the same as the airborne model and is used in WAAS.

$$\sigma_{tropo} = 0.12 \frac{1.001}{\sqrt{0.002001 + \sin^2(el_m)}} \quad \text{m} \tag{A-4}$$

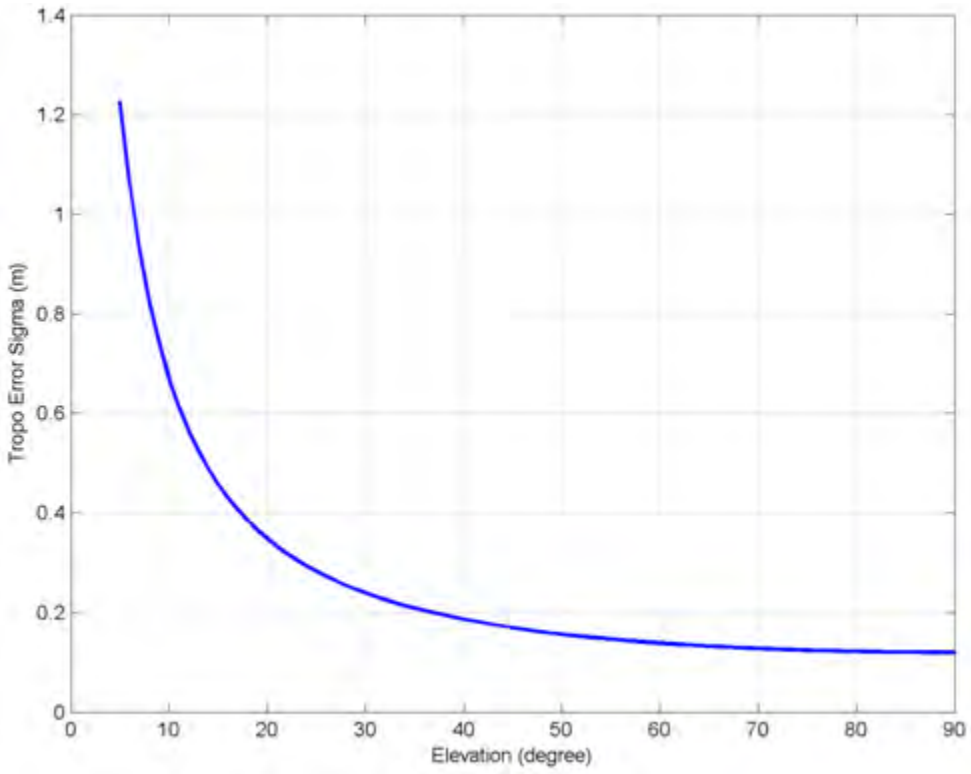

Figure 12 Residual Troposphere Error Standard Deviation

Appendix B Typical SV Ephemeris + Clock Coverage Matrix

B.1 Procedure

A procedure was developed to construct a typical covariance matrix from present GPS SV data. This matrix describes the fault-free ephemeris and clock errors in HCLT coordinates. The PRN31 (Block IIRM) was selected as the representative SV. For the 4 week period of day 1 (June 29) – day 28 (July 26, 2008), PRN31 broadcast ephemeris, clock and precise ephemeris, clock data files were downloaded from the NGA website (**ftp://ftp.nga.mil/pub2/gps/apcpe/2008apc/**).

- The PRN31 position and clock were computed from the broadcast data file using the IS-GPS-200 protocol
- The PRN31 "truth" position and clock were computed from the precise file using the sp3 protocol
- The SV ephemeris and clock errors were then computed at 15 min intervals over the 4 week period
- The resulting ephemeris errors were converted from ECEF to HCLT
- The position and clock errors in HCLT from the 15 min GPS time epochs were interpolated to sidereal 15 min time epochs from day 2 to day 28
- The resulting error data were divided into 28 sidereal day ensemble sections for the computation of ensemble variance and correlation coefficient statistics for the equivalent sidereal time for each day
- The data for each of the four Sundays were discarded due to a software compatibility issue so the actual ensemble sample size is 24 rather than 28.

B.2 Equations

The equation for computing the ensemble variances is

$$\sigma_x^2(k) = \frac{1}{24}\sum_{i=1}^{24}\left[x_i(k) - \bar{x}(k)\right]^2 \qquad \text{(B-1)}$$

$$\bar{x}(k) = \frac{1}{24}\sum_{i=1}^{24} x_i(k) \qquad \text{(B-2)}$$

x: any of the HCLT error components

i: index for sidereal day

k: seconds of week in GPS time for the first sidereal day

The equation for computing ensemble cross-correlation coefficients is

$$\gamma_{xy}(\tau) = \frac{\sum_{i=1}^{24} [x_i(t) - \bar{x}(t)][y_i(t+\tau) - \bar{y}(t+\tau)]}{\sqrt{\sum_{i=1}^{24} [x_i(t) - \bar{x}(t)]^2 \sum_{i=1}^{24} [y_i(t+\tau) - \bar{y}(t+\tau)]^2}} \tag{B-3}$$

x, y: any of the 6 pairs of the HCLT error components

Equation (B-4) represents the typical covariance matrix computed at some time k.

$$\mathbf{C}_0 = \begin{bmatrix} \sigma_h^2 & \gamma_{hc}\sigma_h\sigma_c & \gamma_{hl}\sigma_h\sigma_l & \gamma_{ht}\sigma_h\sigma_t \\ \gamma_{ch}\sigma_c\sigma_h & \sigma_c^2 & \gamma_{cl}\sigma_c\sigma_l & \gamma_{ct}\sigma_c\sigma_t \\ \gamma_{lh}\sigma_l\sigma_h & \gamma_{lc}\sigma_l\sigma_c & \sigma_l^2 & \gamma_{lt}\sigma_l\sigma_t \\ \gamma_{th}\sigma_t\sigma_h & \gamma_{tc}\sigma_t\sigma_c & \gamma_{tl}\sigma_t\sigma_l & \sigma_t^2 \end{bmatrix} \tag{B-4}$$

Figures B-1, B-2 and B-3 are plots of the ensemble standard deviations and cross-correlation coefficients.

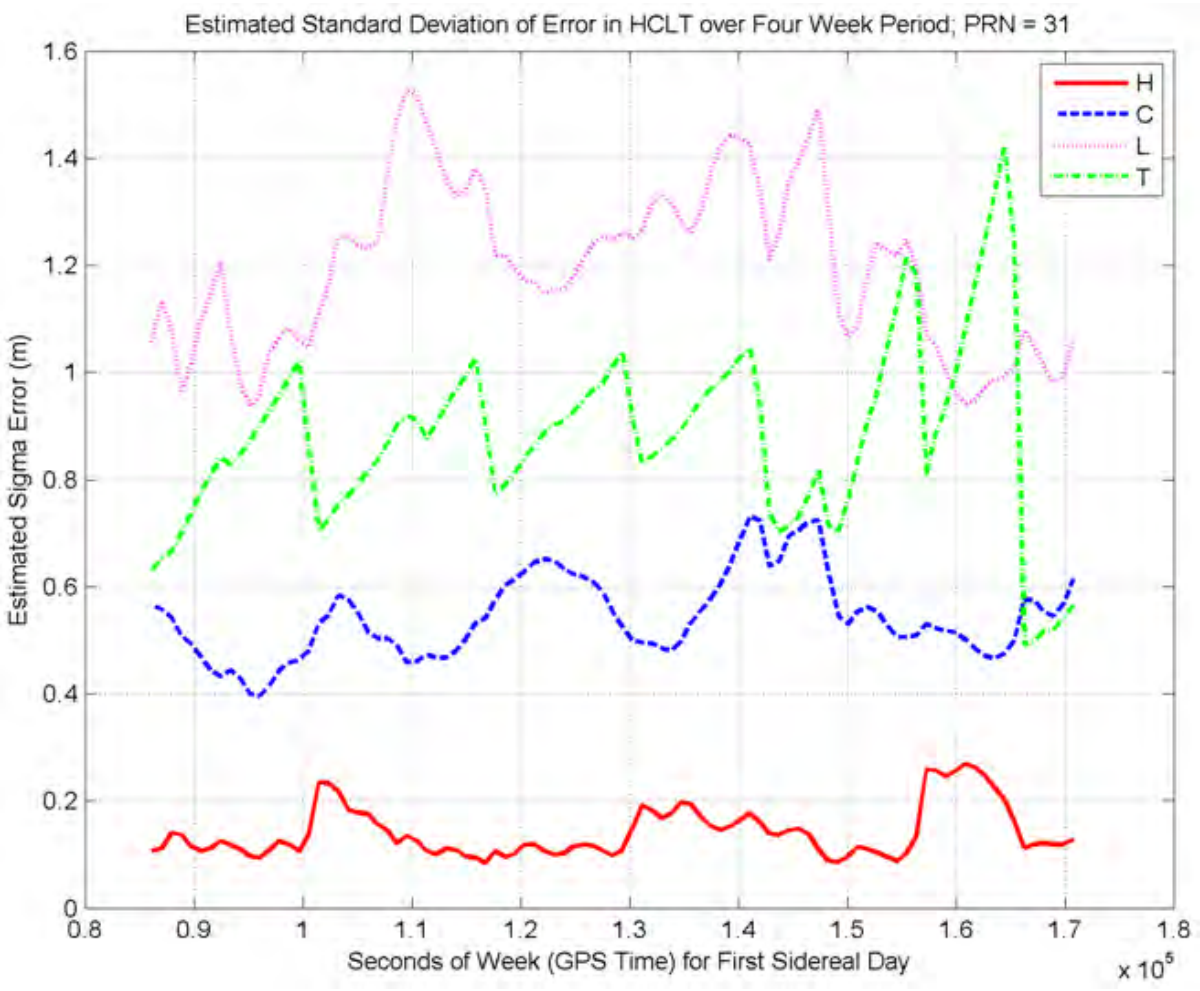

Figure 13 Ensemble Standard Deviations of HCLT Error Components

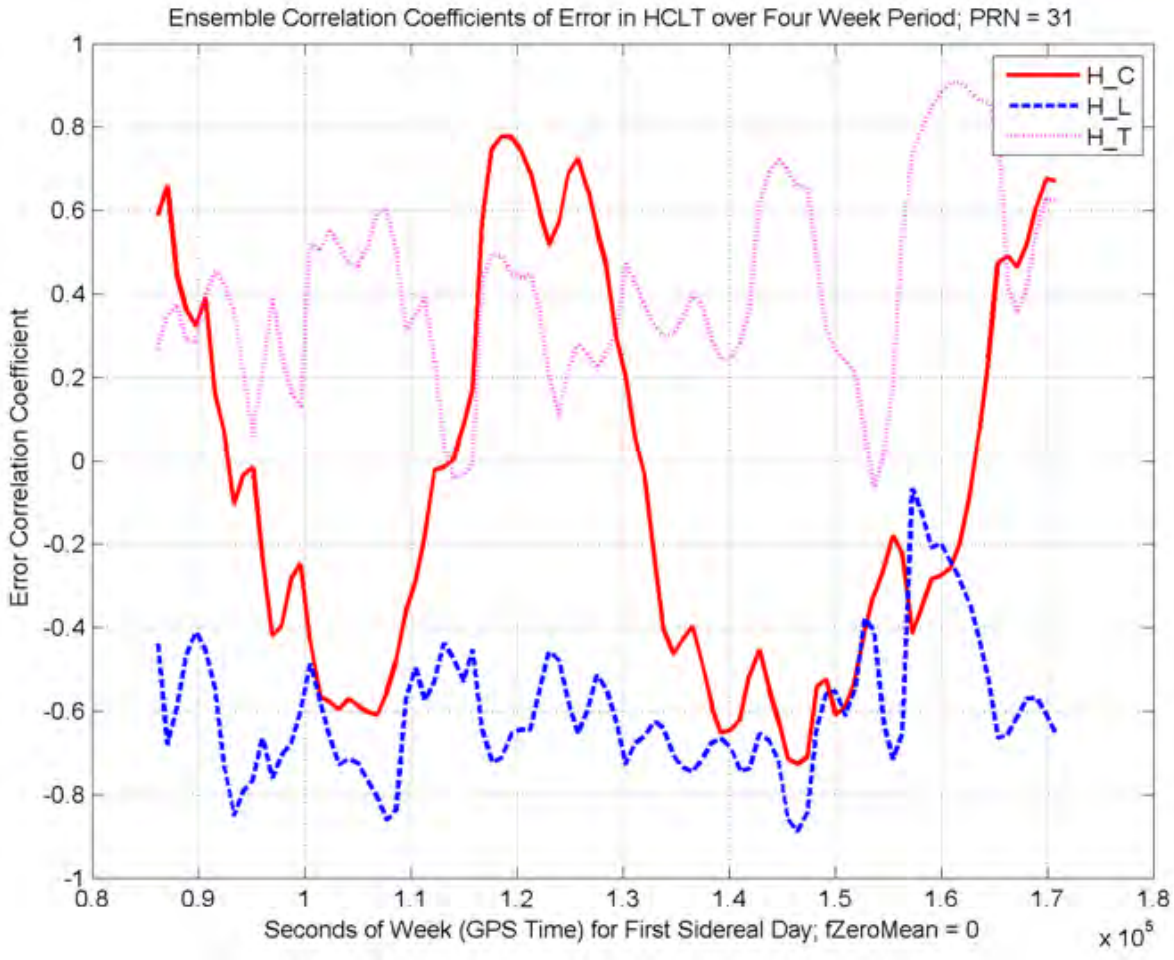

Figure 14 Ensemble Cross-Correlation Coefficients of Components: H_C, H_L, H_T

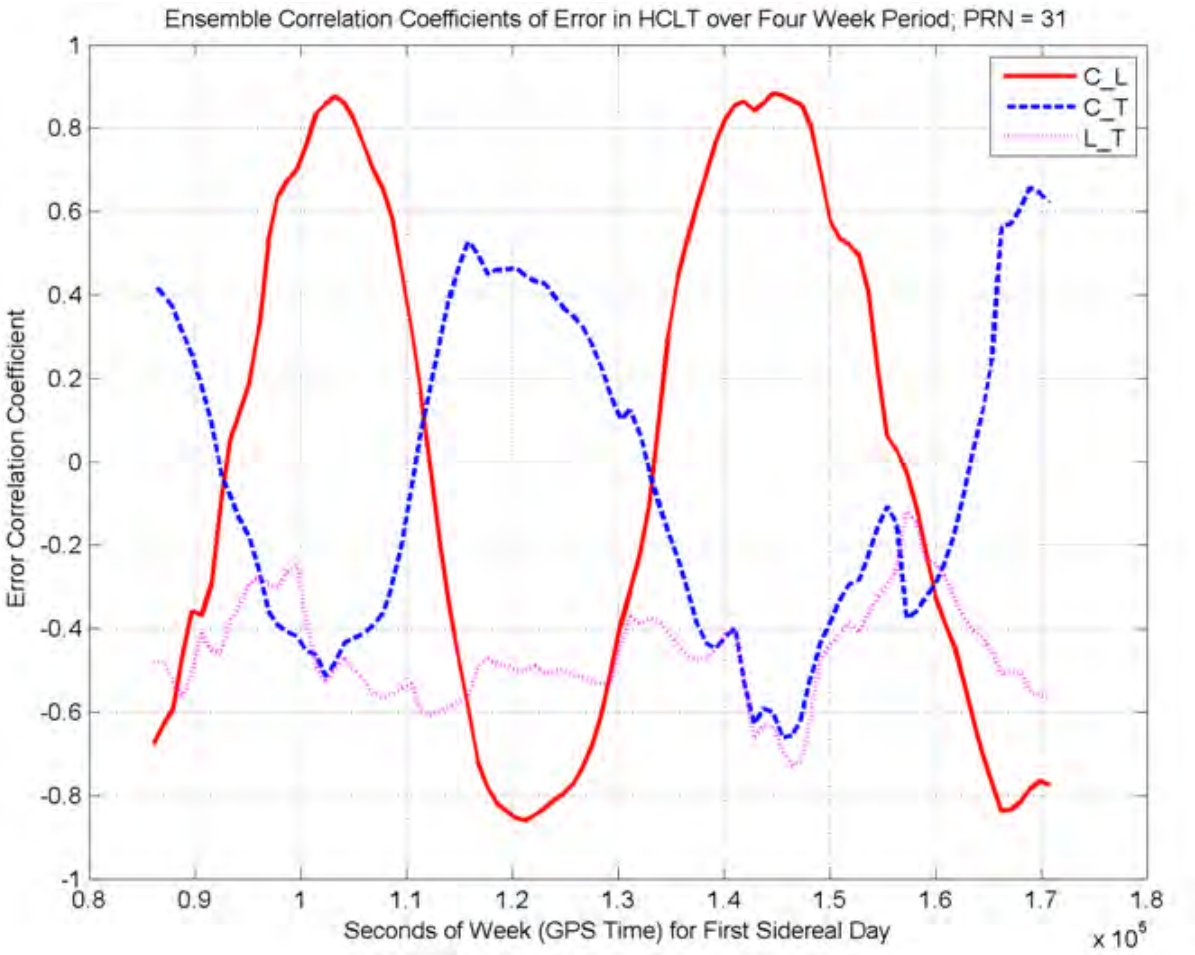

Figure 15 Ensemble Cross-Correlation Coefficients of Components: C_L, C_T, L_T

The typical covariance matrix organized as in (B-4) is computed from the ensemble statistics at time = 1.62×10^5 s on the previous graphs.

$$\mathbf{C}_0 = \begin{bmatrix} 0.0608 & -0.0104 & -0.0820 & 0.2724 \\ -0.0104 & 0.2216 & -0.2415 & -0.0495 \\ -0.0820 & -0.2415 & 0.9456 & -0.4499 \\ 0.2724 & -0.0495 & -0.4499 & 1.5495 \end{bmatrix}$$

Appendix C Over Bounding Justification for RSS

In order to justify the use of RSS, this appendix shows that the probability (P_{ec}) of the SV ephemeris and clock component of a user's range measurement error is bounded by a normal tail probability. That is to show that

$$P_{ec} \le 2 \int_{-\infty}^{-K_I} N(x,0,1)\,dx, \ \forall K_I \tag{C-1}$$

With integrity monitor, P_{ec} is a function of P_{fault} and $P_I\{K_I\, MMU(P_{LOIGF\_req})\}$ given by

$$P_{ec} = P_{fault} \times P_I\{K_I MMU(P_{LOIGF\_req})\} \tag{C-2}$$

Where

$$\begin{aligned} &P_I\{K_I MMU(P_{LOIGF\_req})\} \\ &= \operatorname*{peak}_b \left[\text{prob}\left\{ |e+b| > K_I MMU(P_{LOIGF\_req}) \cap |s+b| \le T_{max} \right\} \right] \\ &= \operatorname*{peak}_b \left\{ \int_{K_I MMU(P_{LOIGF\_req})-b}^{\infty} \int_{-T_{max}-b}^{T_{max}-b} f(s,e)\,ds\,de + \int_{-\infty}^{-K_I MMU(P_{LOIGF\_req})-b} \int_{-T_{max}-b}^{T_{max}-b} f(s,e)\,ds\,de \right\} \end{aligned} \tag{C-3}$$

See (9) for notation definition

Recall from (6), $P_{LOIGF\_req} = 10^{-8} / P_{fault}$. Therefore, $MMU(P_{LOIGF\_req})$ can be considered a function of P_{fault}. Since MMU_{PL} in (16) is the selected MMU, $MMU(P_{LOIGF}) = MMU_{PL}$. In (16), setting $\sigma_{ure} = 0.25$ m, a value of σ_{meas} is calculated to force $MMU_{PL} = 1$ when $P_{fault} = 1$, ($K_{md} = 5.62$ corresponding to $P_{LOIG\_req} = 10^{-8}$). The resulting $\sigma_{meas} = 0.46$ m. The aforementioned values of σ_{meas} and σ_{ure} are substituted into (16) so that $MMU(P_{LOIGF\_req})$ is now only a function of K_{md}. K_{md} is selected to correspond to any desired value of P_{fault}, P_{LOIGF_req}. Table C-1 shows values of K_{md} and resulting $MMU(P_{LOIGF\_req})$ that would be used for values of $P_{fault} = 1, 10^{-2}, 10^{-3}, 10^{-4}$.

Table 9 K_{md} and $MMU(P_{LOIGF\_req})$ Corresponding to P_{fault}

P_{fault}	P_{LOIGF_req}	K_{md} corresponding to P_{LOIGF_req} (1-sided)	$MMU(P_{LOIGF\_req})$
1	10^{-8}	5.62	1 m
10^{-2}	10^{-6}	4.76	0.932
10^{-3}	10^{-5}	4.27	0.893
10^{-4}	10^{-4}	3.72	0.849

Since $MMU(P_{LOIGF\_req})$ has been normalized to unity for $P_{fault} = 1$, the other values of $MMU(P_{LOIGF\_req})$ illustrate their relative reduction due to decreased P_{fault}. To illustrate the range of over bounding as a function of P_{fault}, Figure C-1 contains plots of P_{ec} that show where the over bounding inequality (C-1) is achieved. Over bounding is achieved whenever

P_{ec} is below the Gaussian tail probability in the left figure. The right figure, a plot of the ratio of Gaussian tail probability / P_{ec} versus Gaussian tail probability, indicates over bounding when the ratio ≥ 1. It is seen that over bounding occurs only when $P_{fault} \le 10^{-4}$ / h. (Actually maximum allowable P_{fault} is a value somewhere between 10^{-3} and 10^{-4}.)

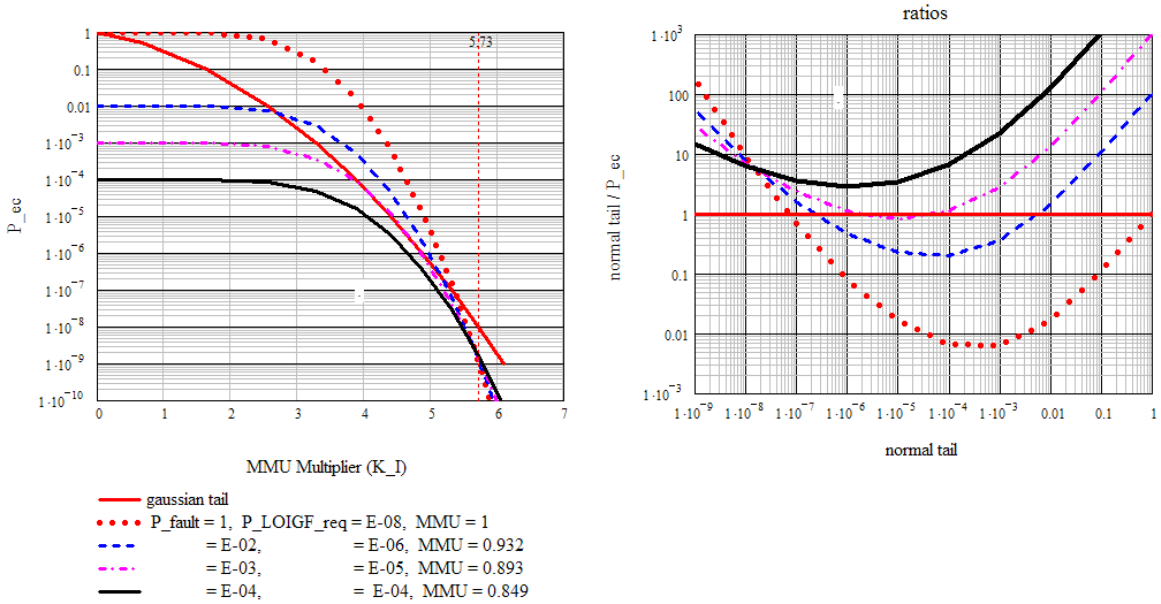

Figure 16 Illustrating Normal Distribution Over Bound for Various Values of P_{LOGIF_req}

It was determined by numerical analysis that the results displayed in Figure C-1 do not change significantly when σ_{meas} or the ratio σ_{ure} / σ_{meas} are varied. Figure C-2 illustrates the variation of P_{ec} as a function of the ratio with the MMU multiplier K_I in (C-2) as the parameter for the case of $P_f = 10^{-4}$, $P_{LOIGF} = 10^{-4}$.

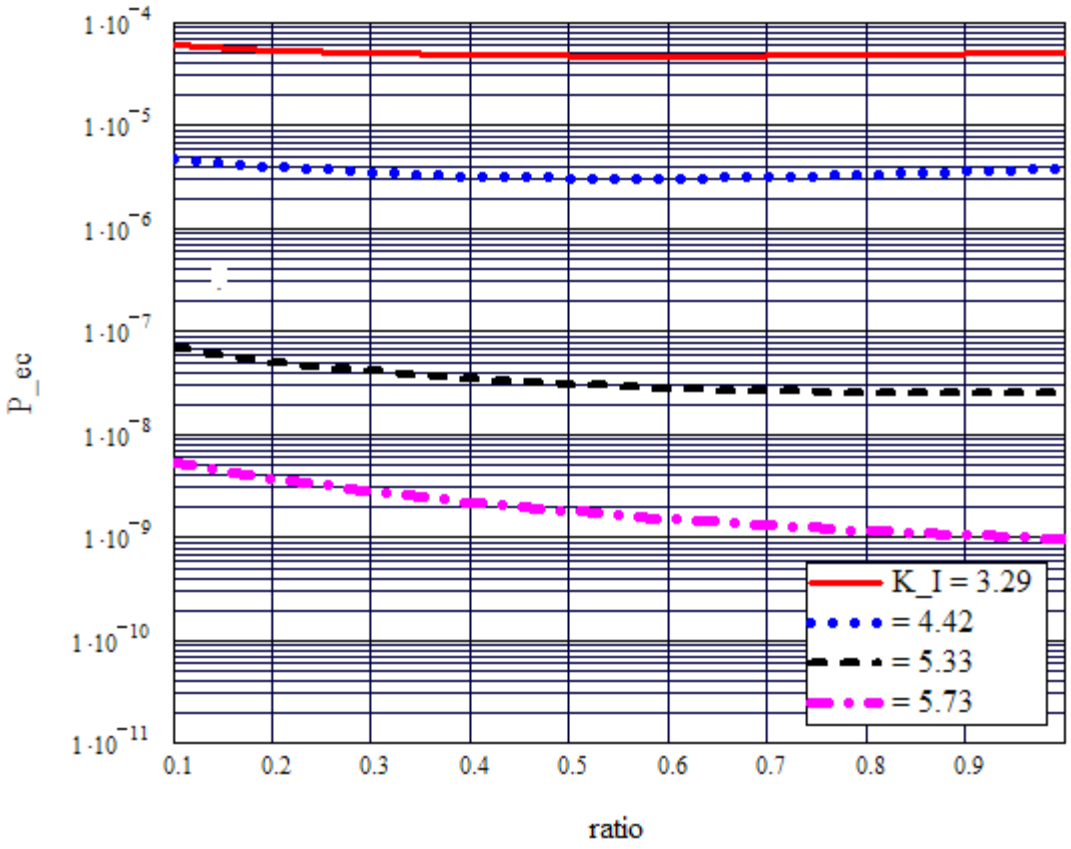

Figure 17 Variation of P_{ec} with Change in Ratio (σ_{ure} / σ_{meas})